AD 745133

INTERIM SCIENTIFIC REPORT

on

ELECTRONIC EFFECTS DUE TO MICRO-INHOMOGENEITIES IN METASTABLE SOLID SOLUTION ALLOYS

E. W. Collings and K. C. Brog

DEPARTMENT OF PHYSICS AND METALLURGY
BATTELLE
Columbus Laboratories

June 23, 1972

This research was supported by the
Air Force Office of Scientific Research
(AFSC) under Grant No. AFOSR-71-2084

DDC
RECEIVED
JUL 19 1972
D

Approved for public release; distribution unlimited.

UNCLASSIFIED

Security Classification

DOCUMENT CONTROL DATA - R & D

(Security classification of title, body of abstract and indexing annotation must be entered when the overall report is classified)

1. ORIGINATING ACTIVITY *(Corporate author)*

Battelle, Columbus Laboratories
505 King Avenue, Columbus, Ohio 43201

2a. REPORT SECURITY CLASSIFICATION

Unclassified

2b. GROUP

3. REPORT TITLE

ELECTRONIC EFFECTS DUE TO MICRO-INHOMOGENEITIES IN METASTABLE SOLID SOLUTION ALLOYS

4. DESCRIPTIVE NOTES *(Type of report and inclusive dates)*

Scientific Interim

5. AUTHOR(S) *(First name, middle initial, last name)*

Edward W. Collings and Kenneth C. Brog

6. REPORT DATE	7a. TOTAL NO. OF PAGES	7b. NO. OF REFS
23 June 1972	39	5

8a. CONTRACT OR GRANT NO	9a. ORIGINATOR'S REPORT NUMBER(S)
AFOSR-71-2084	
b. PROJECT NO: 9761-01	
c. 61102F	9b. OTHER REPORT NO(S) *(Any other numbers that may be assigned this report)*
d. 681306	AFOSR-TR-72-1279

10. DISTRIBUTION STATEMENT

Approved for public release; distribution unlimited.

11. SUPPLEMENTARY NOTES	12. SPONSORING MILITARY ACTIVITY
TECH, OTHER	Air Force Office of Scientific Research 1400 Wilson Boulevard (NE) Arlington, Virginia 22209

13. ABSTRACT

Previously obtained data relating to the magnetic and calorimetric properties of the alloy Ti-Mo (10 at.%) have been analyzed. It was found, on the basis of that work, that "saturated" (metastable equilibrium) ω-phase possessed electronic properties comparable to those of pure α-Ti. As a result we were forced to conclude that such ω-phase precipitates are not themselves inherently brittle, as had been initially expected.

The results of magnetic and calorimetric studies of the systems Ti-Nb and Ti-V are presented. These data have not yet been subjected to detailed analysis.

Finally preprints of papers bearing acknowledgements to OSR, which have been submitted for publication during the year, are attached.

DD FORM 1 NOV 68 1473

UNCLASSIFIED

Security Classification

ELECTRONIC EFFECTS DUE TO MICRO-INHOMOGENEITIES IN METASTABLE SOLID SOLUTION ALLOYS

E. W. Collings and K. C. Brog

DEPARTMENT OF PHYSICS AND METALLURGY
BATTELLE
Columbus Laboratories

June 23, 1972

Approved for public release; distribution unlimited.

Qualified requestors may obtain additional copies from the Defense Documentation Center; all others should apply to the Clearinghouse for Federal Scientific and Technical Information.

TABLE OF CONTENTS

Page

INTRODUCTION 1

SECTION 1

ANALYSIS FOR THE PROPERTIES OF ω-PHASE IN AN AGED Ti-Mo (10 at.%) ALLOY 3

1.1. Normal-State Physical Properties of ω-TM-4.3 7

1.2. Superconductive Properties of ω-TM-4.3 8

1.3. Final Stage of the Analysis Based on Log T_c/Θ_D . . . 11

1.4. Conclusion 14

1.5. References 15

SECTION 2
A. COMPOSITION DEPENDENCE OF PHYSICAL PROPERTIES OF Ti-Nb AND Ti-V ALLOY

EXPERIMENTAL RESULTS FOR Ti-Nb AND Ti-V ALLOYS 16

2.1. Materials Preparation And Heat Treatment 16

2.2. Magnetic Susceptibility of the Ti-Nb and Ti-V Systems 21

2.3. Low-Temperature Specific Heat of the Ti-V System . . 28

2.4. NMR Studies of the Ti-V System 31

B. AGING STUDIES OF A Ti-V (19 at.%) ALLOY

2.5. Magnetic Susceptibility Studies of Aging in Ti-V (19 at.%) 33

2.6. Calorimetric Studies of Aging in TV-19 34

2.7. NMR Studies of Aging in TV-19 36

2.8. Conclusion 38

TABLE OF CONTENTS (Continued)

Page

SECTION 3
MANUSCRIPTS PREPARED DURING THE YEAR

ELECTRONIC EFFECTS DUE TO MICRO-INHOMOGENEITIES IN METASTABLE SOLID SOLUTION ALLOYS

E. W. Collings and K. C. Brog

INTRODUCTION

We introduce this Interim Report by quoting the abstract to our proposal for the first year of research:

> "In the attached research program it is proposed to investigate some basic physical phenomena associated with incipient second-phase precipitation in metastable (i.e., quenched) alloys. In particular, Battelle-Columbus proposes to investigate some bulk electronic effects which have been shown to be associated with ω-phase precipitation in alloys consisting of transition elements dissolved in Ti. Such alloys (i.e., Ti-X alloys) are of great technological interest; however, ω-phase precipitation which often occurs in Ti-rich Ti-X alloys has a severe embrittling effect, rendering the alloy undesirable from a structural standpoint. The embrittling effect of ω-phase should be explainable on an electronic basis in terms of electronic bonding mechanisms. If this view is accepted, an experimental research program designed to investigate fundamental electronic effects in such alloys is quite appropriate.
>
> A study of ω-phase precipitation assumes additional importance when it is realized that the ω-phase is a precursor to clustering, and that local atomic arrangements often dominate the bulk properties of alloys. In this respect the program is important from the standpoint of alloy theory in general. The research program will focus attention on physical electronic effects through the use of "techniques" such as nuclear magnetic resonance, magnetic susceptibility, calorimetry, and electrical resistivity."

During the first year we have made considerable progress towards our goal, that of determining the electronic properties of ω-phase, with a view to understanding its mechanical properties. We are able to conclude, on the basis of experiments and analyses conducted so far, that, although alloys supporting ω-phase precipitation [i.e. (β+ω)-phase alloys] exhibit macroscopic brittleness, the ω-phase itself is <u>not</u> inherently brittle. This situation may be contrasted with that prevailing in concentrated ($\gtrsim$ 15 at.%)

Ti-Al alloys, in which alloy embrittlement can be traced to the presence of brittle, ordered, α_2-phase precipitates within the disordered α-phase matrix.

This result was quite unexpected. We had commenced the program fully expecting to find that the physical properties of ω-phase, when finally extracted, would be characteristic of "poor" (or highly directionally bonded) metals. The analysis of the experimental data for aged Ti-Mo proved otherwise. In fact "saturation" ω-Ti-Mo (4.3 at.%) has physical properties hardly different from those of pure hcp Ti. It must follow that the observed macroscopic embrittlement exhibited by $(\beta+\omega)$-phase alloys is due to a precipitate-matrix interaction. Indeed the results of recent mechanical and optical studies by Williams, Hickman and Marcus* suggest that the immediate cause of embrittlement in $(\beta+\omega)$-phase alloys is microvoid nucleation associated with the nondeformability of the ω-phase particles.

Our conclusions regarding the physical properties of an alloy possessing the ω-phase structure are based on a detailed analysis of the magnetic and superconductive properties of an aged-to-"metastable-equilibrium" Ti-Mo (10 at.%) alloy.

The semi-empirical analytical procedure employed in extracting the fundamental property data is outlined in the first section of this report.

In the second section we present the experimental results obtained so far on the Ti-Nb and Ti-V systems. These data have yet to be subjected to detailed analysis.

Finally we include preprints of four papers, bearing acknowledgments to OSR, which have been submitted for publication during the year.

---

* J. C. Williams, B. S. Hickman and M. L. Marcus, Met. Trans. 2 1913, 1971.

SECTION 1

ANALYSIS FOR THE PROPERTIES OF ω-PHASE IN AN AGED Ti-Mo (10 at.%) ALLOY

The influences of aging at 350° C on the magnetic and calorimetric properties of Ti-Mo (10 at.%) (i.e., TM-10) are shown in Figure 1.1. Quantities depicted are: magnetic susceptibility, χ; electronic-specific-heat coefficient, γ; superconducting transition temperature, T_c; and the Debye temperature, Θ_D. χ, γ, and T_c decrease continuously with aging, while Θ_D behaves in a characteristically inverse manner.

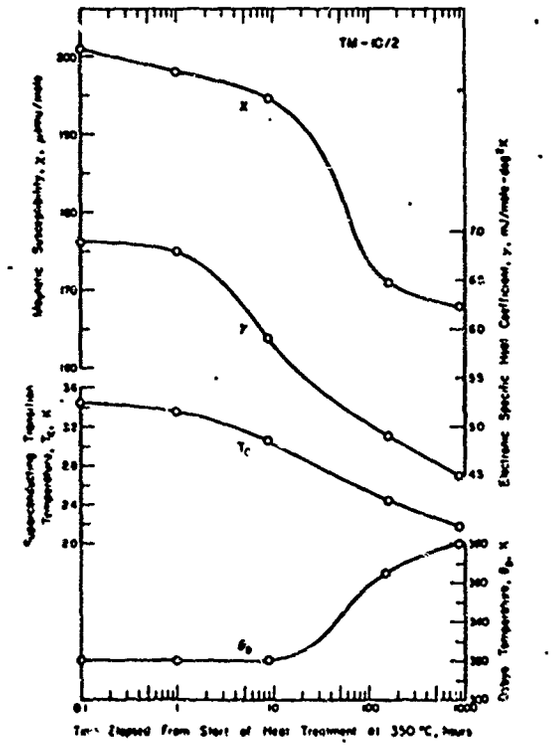

FIGURE 1.1. Influence of aging on the physical properties of the alloy Ti-Mo (10 at.%).

Turning now to Figure 1.2 it is interesting to note that γ, T_c and χ can be imagined to decrease with aging from a set of "ideal" values (half-shaded points) corresponding to single-phase β TM-10--i.e. alloys in which ω-phase precipitation was imagined to have been completely suppressed. The "ideal" data were obtained from curves of γ, T_c and χ corresponding to "virtual β" Ti-Mo as indicated in the inset of Figure 1.2.

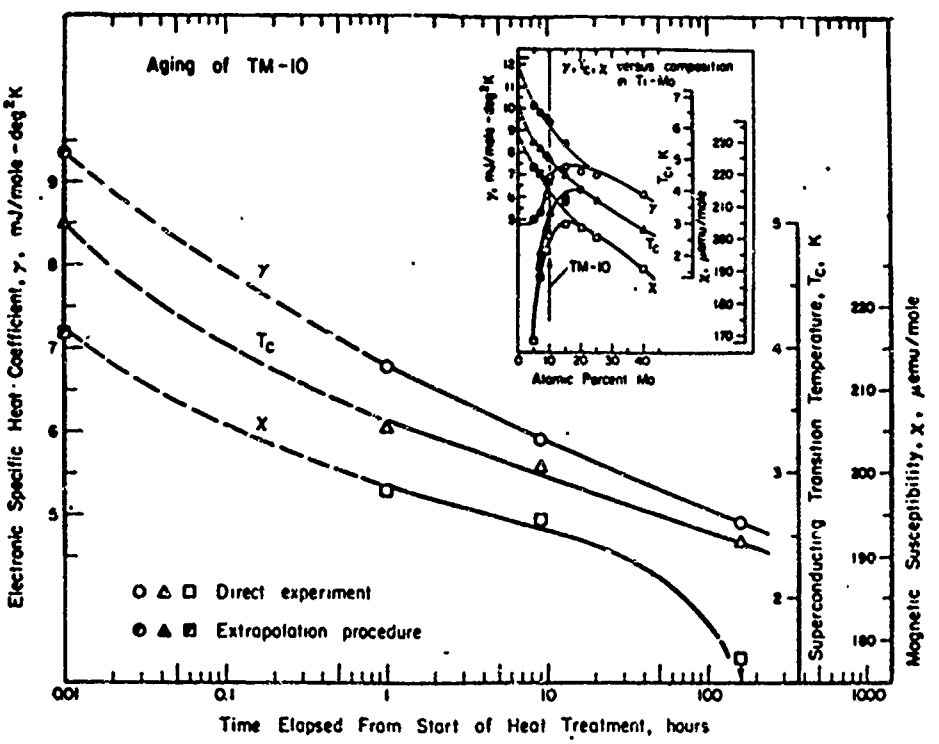

FIGURE 1.2. Monotonic decrease in the physical properties γ, T_c, and χ, with development of ω-phase in Ti-Mo (10 at.%) from an imaginary ideal ω-free initial condition.

In order to determine the electronic properties of ω-Ti-Mo we consider the physical properties corresponding to "saturation-aged" specimens. The results themselves have suggested that 880 hours at 350° C is sufficient to achieve the desired state of metastable (β+ω) equilibrium in TM-10. Referring to the metastable equilibrium phase diagram, Figure 1.3, we first of all point out that the only assumptions made in the following analyses are: (a) that the aging has proceeded to saturation and (b) that the final concentration of Mo in the saturation (or metastable equilibrium) ω-phase is 4.3 at.%. This value was based on the work of Hickman[1]* who suggested 4.3 ± 0.4 at.% Mo; and on our own observations that below a concentration of about 4.5 at.% Mo the α' structure is favored. The input data to the analyses for the physical properties of ω-TM-4.3 are:

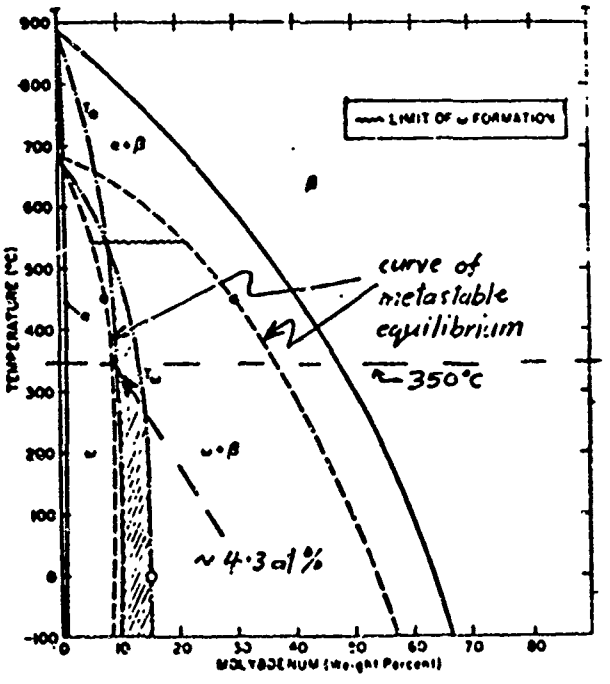

FIGURE 1.3. Metastable equilibrium phase diagram for Ti-Mo. -- after deFontaine et al.[2]

* References are given on page 15.

(a) A Mo concentration in saturated ω-phase at 350° C of 4.3 at.%;

(b) Values of $\langle\chi\rangle_{av}$ $\langle\gamma\rangle_{av}$ $\langle T_c\rangle_{av}$ and $\langle\Theta_D\rangle$ for saturation-aged TM-10;

(c) Values of χ, γ, T_c and Θ_D for single-phase β-Ti-Mo as functions of composition.

The analysis, to be outlined below will yield the following information:

(a) The concentration of Mo in the saturated β component of aged (β+ω)-Ti-Mo at 350° C

(b) Values of χ, γ, T_c and Θ_D for ω-phase TM-4.3.

The experimental input data are listed in Table 1.1.

TABLE 1.1. PHYSICAL PROPERTIES OF A FULLY-AGED (350°C) Ti-Mo (10 at.%) ALLOY

Physical Property	Measured Value After Aging
Magnetic Susceptibility, χ, μ emu/mole	167.9
Electronic-Specific-Heat Coefficient, γ, mJ/mole-deg^2	4.5_5
Superconducting Transition Temperature, T_c, kelvins	380
Debye Temperature, Θ_D, kelvins	$2.1_8 \pm 0.1_0$

1.1. Normal-State Physical Properties of ω-TM-4.3

The starting point for the numerical analysis is the "conservation equation":

$$\langle\Phi\rangle_{av} = f_\omega \Phi_\omega + (1-f_\omega) \Phi_\beta , \qquad (1)$$

where Φ represents a molar physical property, and f_ω is the mole-fraction of ω-phase present in the saturated (β+ω) alloy.

The first step in the analysis follows when we write $\Phi \equiv$ [Mo]; in which case Equation (1) corresponds to the well-known "lever rule". As mentioned earlier, our initial assumption is that $[Mo]_\omega$ = 4.3 at.%. It is, therefore, possible to derive the concentration of Mo in the β-component (i.e., $[Mo]_\beta$) as a function of f_ω = 0.49, 0.55, 0.60, 0.65, 0.70, and 0.75.

Next, with $\Phi \equiv \chi$, γ, and Θ_D, in turn; and knowing the values of χ_β, γ_β and $\Theta_{D,\beta}$ for all concentrations of β-Ti-Mo, reapplications of the conservation equation yield:

$\left.\begin{array}{l}\chi_\omega \\ \gamma_\omega \\ \Theta_{D,\omega}\end{array}\right\}$ as functions of f_ω, within the above-mentioned range of 0.49-0 75.

These values, together with $[Mo]_\beta$ are plotted in Figure 1.4. So far the required physical property values are indeterminate, since the actual value of f_ω has not yet been selected.

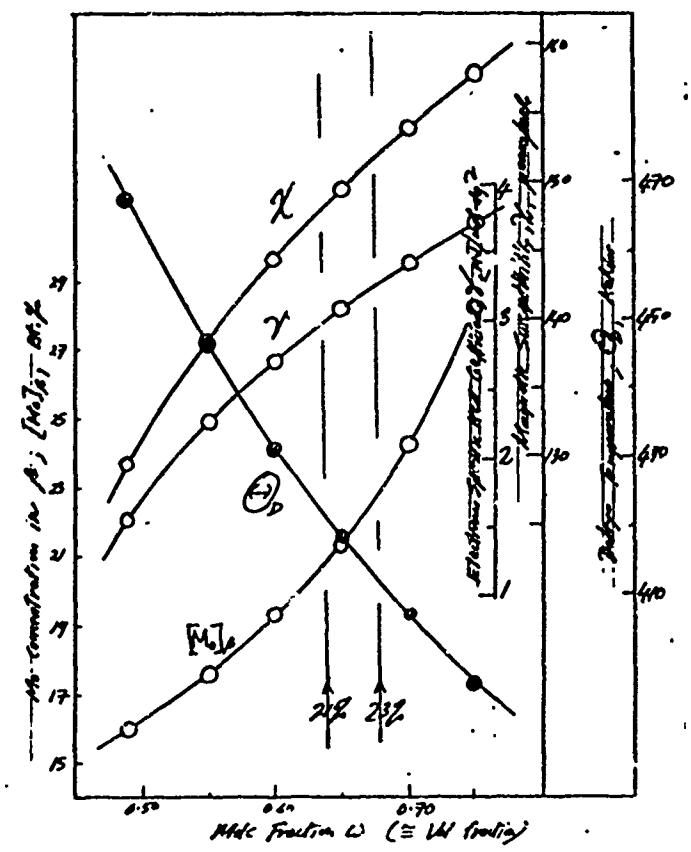

FIGURE 1.4. Physical quantities χ_ω, γ_ω, $\Theta_{D,\omega}$, and $[Mo]_\beta$ plotted as functions of the mole-fraction of ω-phase present at metastable equilibrium in Ti-Mo (10 at.%) (f_ω).

1.2. Superconductive Properties of ω-TM-4.3

The superconducting transition temperature is treated using a different form of conservation equation. For a system of two components in close proximity $\langle T_c \rangle_{av}$ is influenced by:

(a) The T_c of each component;

(b) The relative volumes of each component participating in the superconductivity. Here the penetration depth of electron pairs (the coherence length, ξ_o) into the lower-T_c material plays an important role.

(c) The Fermi density-of-states, $n(E_F)$, in the two materials. In the $(\beta+\omega)$ alloys we have an interesting situation in which the ω-phase particles are practically completely penetrated by the superconductive electron-pair wave-functions--Figure 1.5. Because of this the volume fractions of β and ω participating in the superconducting transition are the actual volume fractions physically present in the specimen.

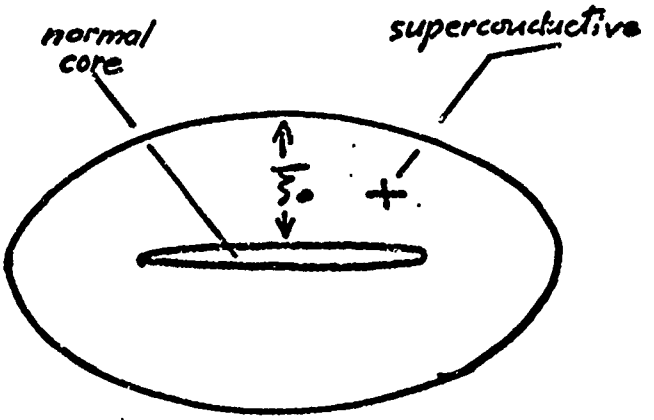

FIGURE 1.5. In TM-10 we estimate the ellipsoidal ω-phase particles to be practically completely penetrated by the superconducting electrons.

At this stage we make the simplifying assumption that the volume-fraction of ω-phase is practically the same as the mole-fraction; i.e., $v_\omega \equiv f_\omega$.

The proximity-effect expression employed is

$$\langle T_c \rangle_{av} = \frac{\sum_{\omega}^{\beta} v.n(E_F).T_c}{\sum_{\omega}^{\beta} v.n(E_F)} . \qquad (2)$$

For substitution in this expression, an $n(E_F)$ can be derived from γ itself. All the relevant physical properties of ω-phase, except T_c, have just been derived as functions of f_ω (hence [Mo]); and the physical properties of β-Ti-Mo are also known, as a result of previous work. The unknown in Equation (2) is, therefore, $T_{c,\omega}$ which we can now calculate as a function of f_ω. The results of the calculation, along with the previously derived physical properties, are displayed in Figure 1.6. Referring to this Figure, it would be safe to guess that $T_{c,\omega}$ lies between 0 and 1K. If so, f_ω would take on values between 0.63 and 0.71; a physically realistic range.

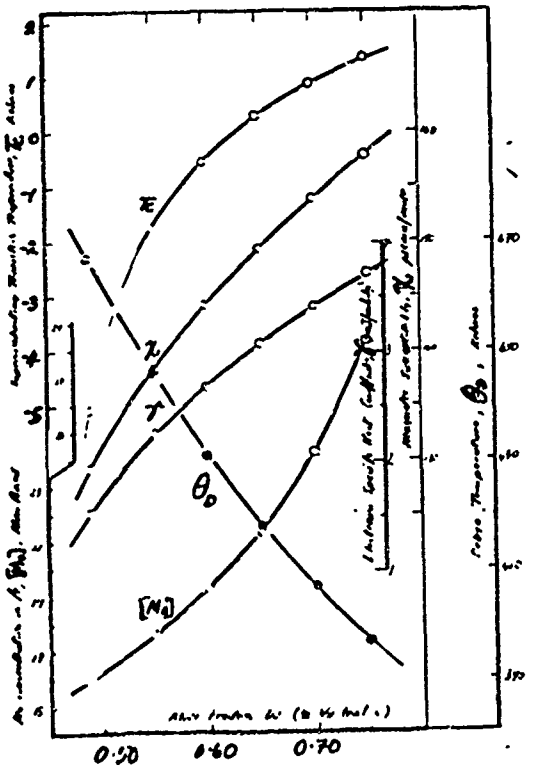

FIGURE 1.6. Superconducting transition temperature T_c plotted versus f_ω; together with the previously calculated quantities γ_ω, χ_ω, $\Theta_{D,\omega}$ and $[Mo]_\beta$.

The desired physical parameters of ω-Ti-Mo (4.3 at.%), for f_ω between 0.64 and 0.68 are shown in Table 1.2.

TABLE 1.2. PHYSICAL PROPERTY PARAMETERS OF ω-PHASE Ti-Mo (4.3 at.%)

At.% Mo in β	21	22	23
Physical Property of ω-TM-4.3			
f_ω	0.64	0.66	0.68
T_c	0.2_0	0.4_6	0.7_0
γ	3.0_0	3.1_5	3.2_9
χ	148.5	150.4	152.1
Θ_D	420	416	411

1.3. Final Stage of the Analysis Based on Log T_c/Θ_D

By taking one additional step it is possible to arrive at the physical state of ω-Ti-Mo (4.3 at.%) with considerable accuracy and reliability. In previously published work we have noted[3] that the measured data points for both β and (β+ω) alloys, as well as hcp Ti, all lie close to a straight line, when plotted in the format log T_c/Θ_D *versus* $1/0.21^2\gamma$. It, therefore, seems reasonable that ω-TM-4.3 should also be represented by a point on that line. This approach enables us to select a value for $[Mo]_\beta$ (or f_ω) from among the three listed in Table 1.2, since T_c varies quite rapidly with f_ω in the range $0.64 \leq f_\omega \leq 0.68$.

For insertion in a plot of log T_c/Θ_D versus $1/0.212\ \gamma$, we assemble the experimental data in the manner of Table 1.3. Because of the rapidity

TABLE 1.3. PARAMETERS FOR ω-PHASE Ti-Mo (4.3 at.%) FOR INSERTION IN THE SEMI-LOG PLOT OF FIGURE 1.7

At.% Mo in β	21	22	23
Physical Property of ω-TM-4.3			
T_c/Θ_D	0.00047_6	0.0011	0.0017
$1/0.212\ \gamma$	1.57	1.50	1.43

with which T_c varies with f_ω (Figure 1.7) we feel confident in assigning the value $[Mo]_\beta$ = 21 at.%. It follows that the physical properties of ω-TM-4.3 we seek are those listed in the first column of Table 1.4.

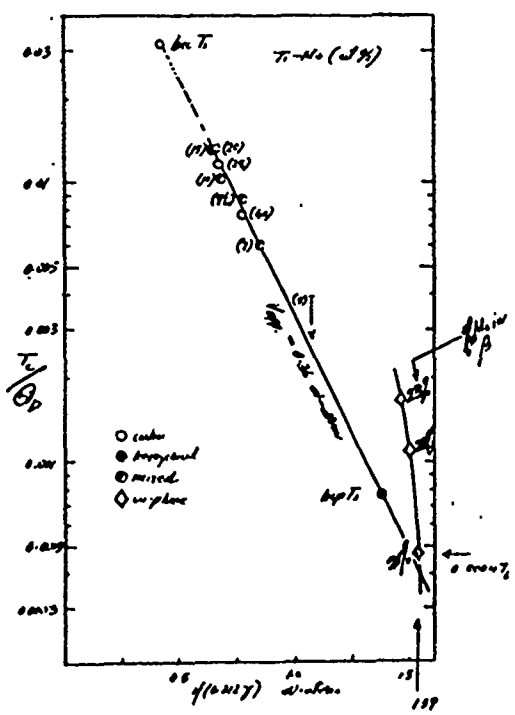

FIGURE 1.7. Plot of log (T_c/Θ_D) versus $(0.212\ \gamma)^{-1}$. The points corresponding to low $(T_c/\Theta_D)]_\omega$ are shown. The best fit is obtained for $[Mo]_\beta$ = 21 at.%.

It is instructive to compare this set of values with other relevant data for Ti-Mo. Firstly we note that the value of 21 at.% for $[Mo]_\beta$ is very close to that value for $[Mo]_\beta$ (350° C) prescribed by the metastable equilibrium ($\beta+\omega$) phase diagram of de Fontaine et al.[2] (Figure 1.3). Secondly we see that the values of χ_ω, γ_ω, $T_{c,\omega}$, and Θ_D, so derived, are able to terminate nicely the corresponding curves for ($\beta+\omega$)-Ti-Mo obtained from the results of magnetic and calorimetric experiments on the quenched alloys--Figure 1.8.

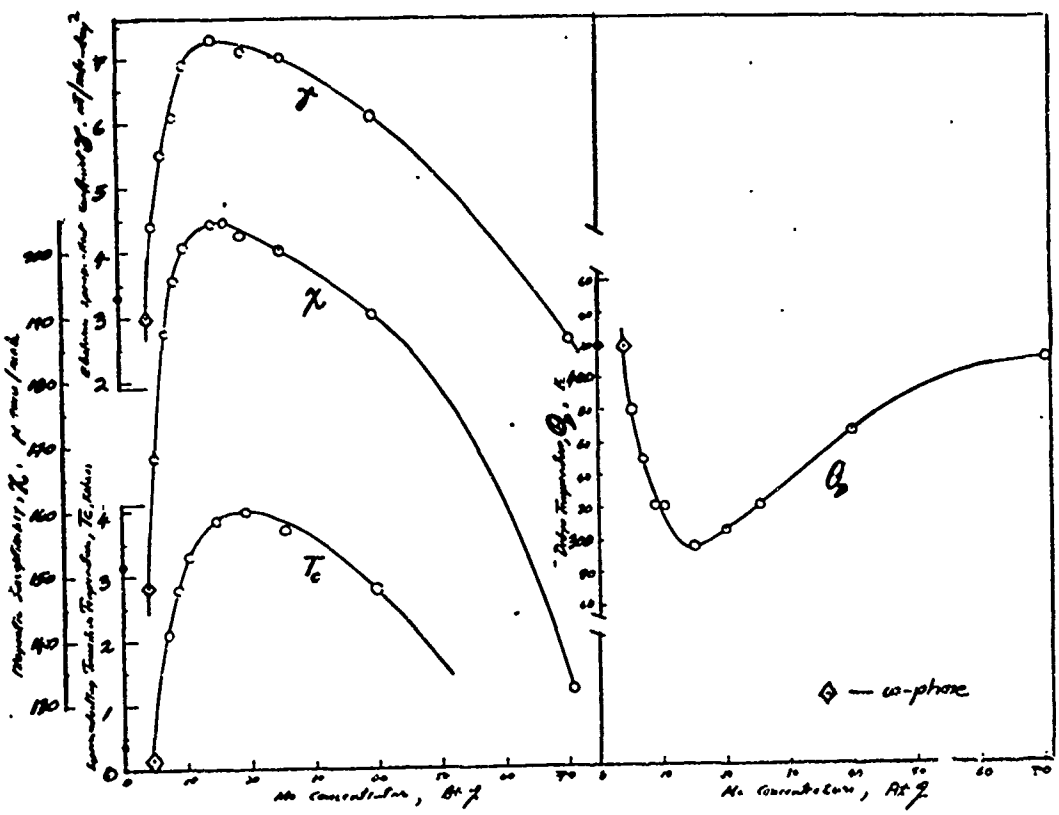

FIGURE 1.8. Physical properties γ, χ, T_c and Θ_D as functions of composition in Ti-Mo. The points corresponding to ω-TM-4.3 fit nicely on extensions of the descending ($\beta+\omega$) portions of the curves.

1.4. Conclusion

Based on the preceding analyses we are able to derive important information dealing with

(a) Metastable phase equilibria in aged Ti-Mo

(b) The physical properties and, hence, mechanical characteristics of ω-TM-4.3.

With regard to the former, an appropriate analysis of the results of aging experiments yields a metastable equilibrium phase diagram.

With regard to the latter, we note in Figure 1.8 that the physical properties of ω-TM-4.3 are very close to those of pure Ti. It follows from arguments presented elsewhere,[4] regarding the relationships between electronic and mechanical properties of Ti alloys, that the mechanical properties ω-TM-4.3 should not differ greatly from those of pure Ti. As a particular example, the extreme brittleness known to be associated with the α_2 precipitated particles in concentrated $(\alpha+\alpha_2)$-Ti-Al alloys should not be a characteristic shared by ω-TM-4.3. Indeed the results of the mechanical property studies of Williams, Hickman and Marcus[5] substantiate this view.

1.5. References

(1) B. S. Hickman, Trans. Met. Soc. AIME 245 1329 (1969).

(2) D. De Fontaine, N. E. Paton, and J. C. Williams, Acta. Met. 19 1153 (1971).

(3) E. W. Collings and J. C. Ho, Proceedings of the 3rd Materials Research Symposium, November, 1969, "Electronic Density of States", Ed. L. M. Bennett, Nat. Bur. Stand. (U.S.) Special Publication 323, December, 1971, p. 587.

(4) E. W. Collings, J. E. Enderby, H. L. Gegel, and J. C. Ho in "Some Relationships Between the Electronic and Mechanical Properties of Ti Alloys, Discussed From the Standpoint of Fundamental Alloy Theory"--Proceedings of the Second International Conference on Titanium, Boston, Mass., May 2-5, 1972.

(5) J. C. Williams, B. S. Hickman, and M. L. Marcus, Met. Trans. 2 1913 (1971).

SECTION 2
A. COMPOSITION DEPENDENCE OF PHYSICAL PROPERTIES OF Ti-Nb AND Ti-V ALLOY

EXPERIMENTAL RESULTS FOR Ti-Nb AND Ti-V ALLOYS

In this section we present some of the experimental results of our magnetic and calorimetric investigations of Ti-Nb and Ti-V alloys. These data have not yet been subjected to detailed analysis.

2.1. Materials Preparation And Heat Treatment

Alloys were prepared by arc melting from high-purity ingredients obtained from the following suppliers:

Titanium, "Grade ELXX": Titanium Metals Corporation

Vanadium, "VP Grade": Materials Research Corporation

Niobium, "VP Grade": Materials Research Corporation.

Typical analyses of the starting materials are listed in Table 2.1.

TABLE 2.1

(a) Titanium Typical Analysis

Impurity	Wt., Pct.	Impurity	Wt., Pct
N	0.003	Mo	<0.001
C	0.010	Al	<0.001
Cl	0.059	V	<0.001
H	0.003	Sn	<0.02
O	0.041	Mn	<0.001
H_2O	0.008	Ni	0.005
Si	0.002	Cu	<0.001
Na	0.022	Mg	<0.001
Fe	<0.001	Zr	<0.001
Cr	0.006	B	<0.001

(b) Vanadium - Typical Analysis

Impurity	Wt., ppm	Impurity	Wt., ppm
C	20.0	Mo	3.0
H	3.0	Na	ND
O	300.0	Nb	2.0
N	20.0	Ni	15.0
Ag	1.0	P	2.0
Al	0.1	Pb	1.0
As	ND	Pd	<1.0
B	ND	Pt	ND

TABLE 2.1. (Continued)

Impurity	Wt., ppm	Impurity	Wt., ppm
Bi	ND	Rh	ND
Ca	0.3	Ru	ND
Cd	ND	S	5.0
Co	1.0	Si	ND
Cr	ND	Sn	ND
Cu	10.0	Ta	1.0
Fe	70.0	Ti	ND
Hf	ND	W	20.0
Ir	ND	Zn	1.0
K	0.1	Zr	1.0
Mg	1.0	Mn	0.5

(c) Niobium - Typical Analysis

Impurity	Wt., ppm
C	25
O	50
N	15
H	15
B	<10
Mg	<10
Al	5
Si	<10

TABLE 2.1. (Continued)

Impurity	Wt., ppm
Ca	5
Ti	<10
Cr	<10
Mn	<10
Fe	25
Co	<10
Ni	<10
Cu	<10
Zr	50
Mo	50
Sn	<10
Ta	500
W	<100
Hf	100

Specimens were removed from the arc-melted buttons according to the following prescriptions:

(a) Specific-Heat Specimens - 30g piece

(b) Magnetic-Susceptibility Specimen - 100-200 mg cube

(c) Electron-Microscopy Specimens - 3/4-inch diameter, thin disc

(d) NMR Material - fine powder.

Although some measurements were made on as-cast material most of the studies come carried out on alloys which had been quenched into iced brine following an anneal usually for 1 hour at 1000° C. In preparation for this heat treatment the material was encapsulated in vycor envelopes under 1/2 atm. Ar according to the scheme summarized in Figure 2.1.

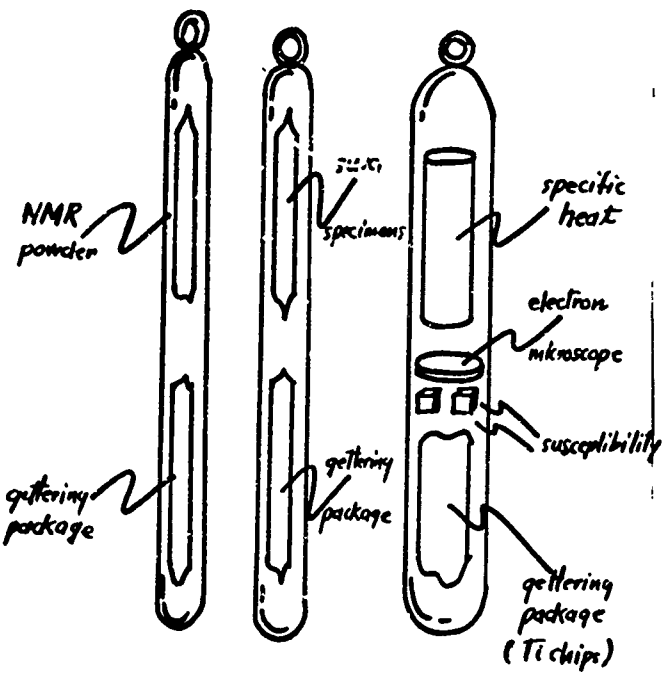

FIGURE 2.1. Encapsulation of specimens in vycor tubes for heat treatment (1 hr at 1000°C) and quenching in iced brine.

Prior to the anneal, the getter was activated in the induction unit. Typically four packages of each kind were prepared to accommodate the aging schedule outlined in Table 2.2.

TABLE 2.2. AGING SCHEME

[Approximate Times (hr) at 300°C]

Capsule 1	1 → 5 → 10 → 20 (specimen reencapsulated between agings)
Capsule 2	100
Capsule 3	300
Capsule 4	1000

2.2. Magnetic Susceptibility of the Ti-Nb and Ti-V Systems

Magnetic susceptibility was measured by the Curie Technique; magnetic forces being measured at each of 5 magnetic field strengths to enable a correction for possible ferromagnetic contamination to be applied. The following Table and subsequent magnetic susceptibility tables, list the extrapolated (infinite field) values of magnetic susceptibility.

The data of Tables 2.3(a to d) are plotted in Figures 2.2 and 2.3.

TABLE 2.3(a). MAGNETIC SUSCEPTIBILITY OF Ti-Nb - AS-CAST

Nominal Composition (at.%)	Magnetic Susceptibility (μ emu/g)	Magnetic Susceptibility (μ emu/mole)
0	3.17	151.84
5	3.198	160.41
10	3.240	169.78
15	2.976	162.67
20	3.362	191.30
22	3.422	197.79
25	3.393	200.73
30	3.544	217.60
40	3.392	223.53
50	3.056	215.17
60	2.881	215.82
70	2.707	214.96
100	2.306	214.25

TABLE 2.3(b). MAGNETIC SUSCEPTIBILITY OF Ti-Nb - QUENCHED

Nominal Composition (at.%)	Magnetic Susceptibility (μ emu/g)	Magnetic Susceptibility (μ emu/mole)
0	3.17	151.84
5	3.214	161.21
10	3.248	170.20
15	2.996	163.76
20	3.396	193.23
22	3.454	199.64
25	3.394	200.79
30	3.588	220.30
40	3.410	224.72

TABLE 2.3(b). (Continued)

Nominal Composition (at.%)	Magnetic Susceptibility (μ emu/g)	Magnetic Susceptibility (μ emu/mole)
50	3.056	215.17
60	2.880	215.74
70	2.699	214.33
100	2.306	214.25

TABLE 2.3(c). MAGNETIC SUSCEPTIBILITY OF Ti-V - AS-CAST

Nominal Composition (at.%)	Magnetic Susceptibility (μ emu/g)	Magnetic Susceptibility (μ emu/mole)
0	3.17	151.84
3	3.371	161.77
6	3.565	171.44
	3.588	172.55
9	3.769	181.59
10.5	3.878	187.00
12	3.667	176.97
15	3.926	189.86
15(a)	3.943	190.68
	3.946	190.83
	3.955	191.26
	3.910	189.09
	3.940	190.54
	3.933	190.20
19(a)	4.380	212.34
	4.384	212.54
20	4.478	217.23

TABLE 2.3(c). (Continued)

Nominal Composition (at.%)	Magnetic Susceptibility (μ emu/g)	Magnetic Susceptibility (μ emu/mole)
25	4.856	236.34
30	4.953	241.81
40	5.111	251.05
50	5.215	257.78
60	5.338	265.46
70	5.424	271.42
90	5.617	284.50
	5.592	283.23
100		
	5.611	285.88
	5.603	285.47

(a) "Finger" ingot - all the others were ~50g "buttons".

TABLE 2.3(d). MAGNETIC SUSCEPTIBILITY OF Ti-V - QUENCHED

Nominal Composition (at.%)	Magnetic Susceptibility (μ emu/g)	Magnetic Susceptibility (μ emu/mole)
0	3.17	151.84
3	3.405	163.41
6	3.611	173.65
	3.581(a)	172.21
9	3.783	182.26
10.5	3.844	185.36
	3.843	185.31
12	3.633	175.33
15	3.93	190.05
15(b)	3.881	187.69
	3.870	187.15

TABLE 2.3(d). (Continued)

Nominal Composition (at.%)	Magnetic Susceptibility (μ emu/g)	Magnetic Susceptibility (μ emu/mole)
19(b)	4.526	219.42
	4.497	218.01
	4.425(c)	214.52
	4.407(c)	213.65
20	4.475	217.08
25	4.813	234.25
30	4.956	241.95
40	5.088	249.92
	5.132	252.08
	5.090(d)	250.02
50	5.225	258.27
	5.276	260.79
	5.239(d)	258.96
60	5.359	266.50
	5.405	268.79
	5.402(d)	268.64
70	5.433	271.87
	5.454	272.92
80	5.605	282.16
	5.604(d)	282.11
100	5.611	285.88
	5.603	285.47

(a) As-cast plus 400 hr at 600° C.

(b) "Finger" ingot - all the others were ~ 50g "buttons".

(c) Quenched plus 12 days at room temperature.

(d) Quenched plus 1/2 hr at 900° C - furnace cool (strain-relieving treatment).

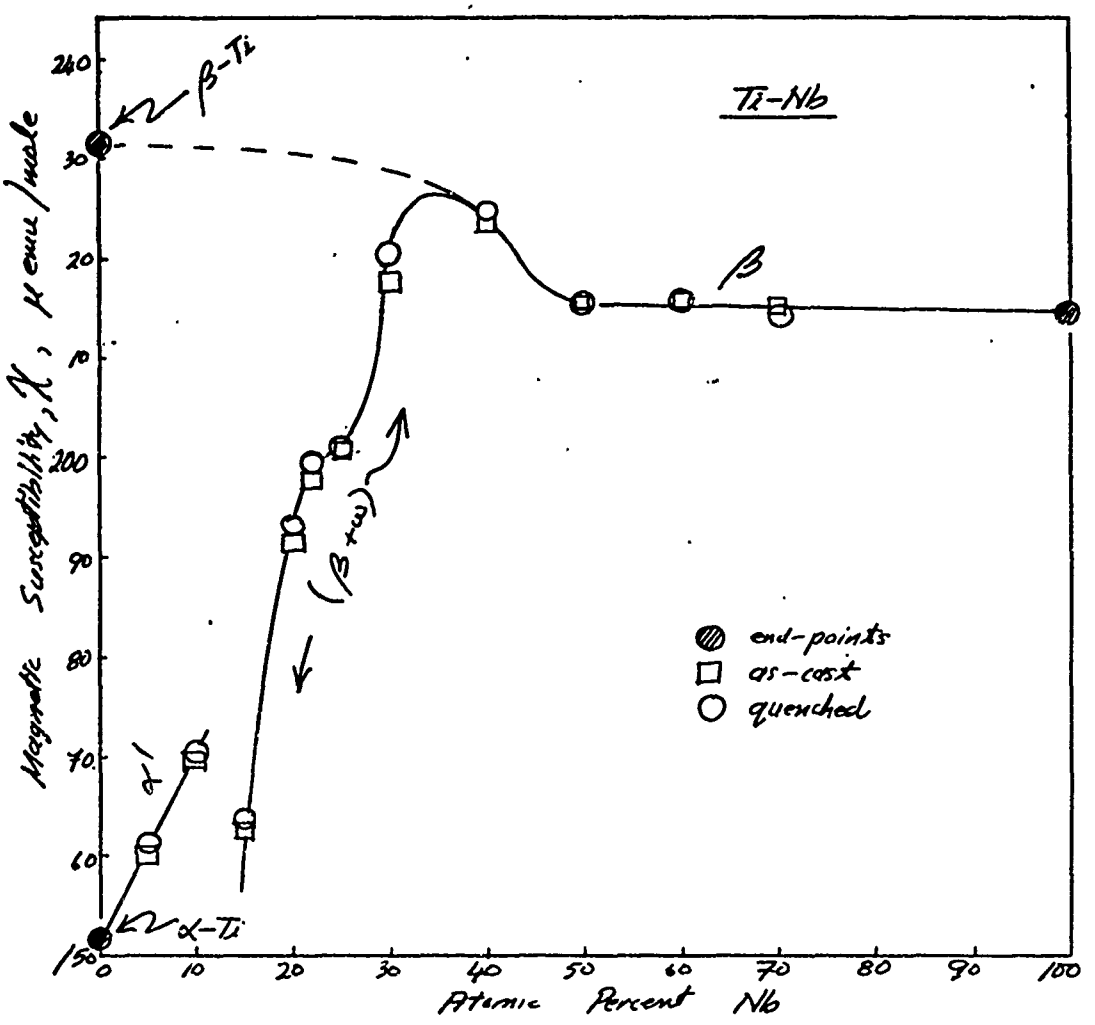

FIGURE 2.2. Composition-dependence of magnetic susceptibility of Ti-Nb in both as-cast and quenched conditions.

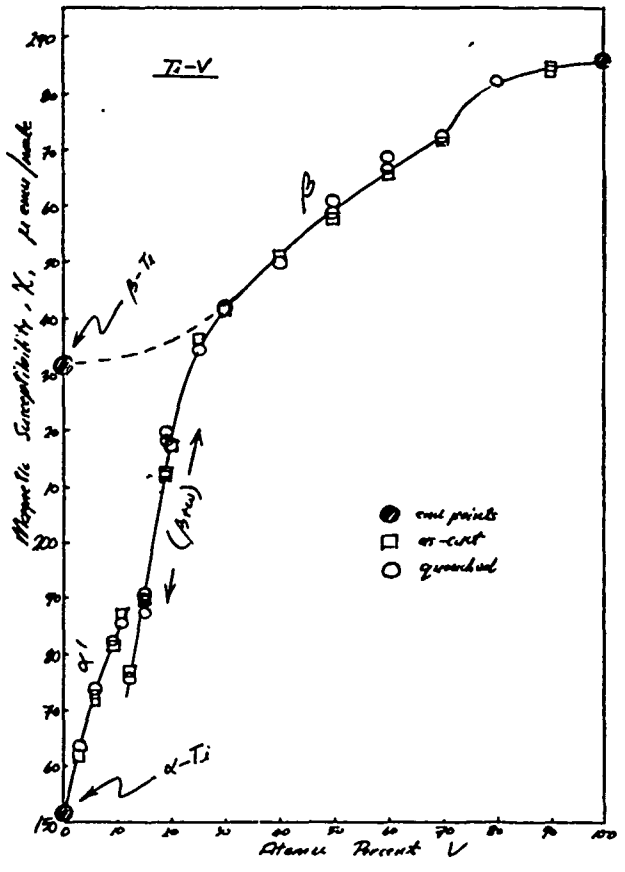

FIGURE 2.3. Composition-dependence of magnetic susceptibility of Ti-V in both as-cast and quenched conditions.

Referring to both Figures 2.2 and 2.3 we see a pronounced discontinuity at the $\alpha'/(\beta+\omega)$ phase boundary, followed by a rapid increase in χ with solute concentration as the volume-fraction of ω-phase present in the alloys decreases. Referring to the direction of <u>decreasing</u> solute concentration, we suggest that χ would continue as an extrapolation of the β-phase $\chi(c)$ curve (dashed line) if ω-phase precipitation did not intervene to reduce the average total susceptibilities.

2.3. Low-Temperature Specific Heat of the Ti-V System

Low-temperature specific heat was measured in the temperature range 1.5 to 6K using a simple adiabatic calorimeter. The calorimetric technique, applied to a superconductive material yields a wealth of useful information viz:

(a) γ, the electronic specific-heat coefficient, which when suitably corrected yields the electronic density-of-states at the Fermi level.

(b) Θ_D, the Debye temperature.

(c) T_c, the superconducting critical temperature.

(d) $C_{es}/\gamma T_c$, the relative height of he specific-heat jump at T_c, from which it is possible to determine whether or not a bulk superconducting transition is involved.

The output from the experimental apparatus is analyzed and displayed in the format C/T versus T^2. A typical plot is shown in Figure 2.4.

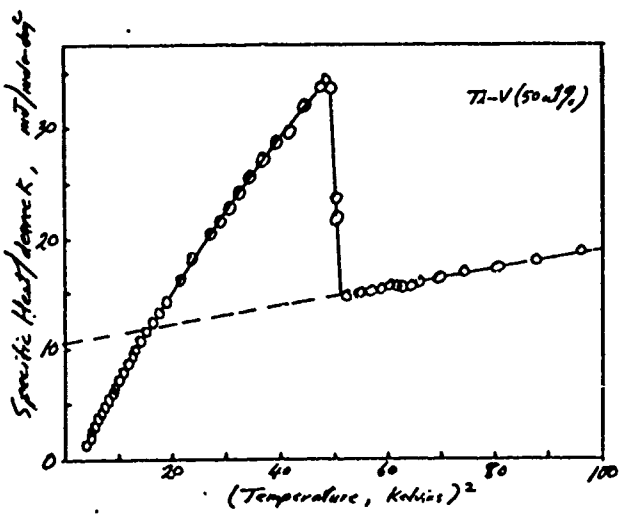

FIGURE 2.4. Typical low-temperature "specific heat plot" in the format C/T versus T^2. The curve exhibits a characteristic superconductive jump.

The intercept yeilds γ, the slope yields Θ_D, and the specific-heat jump occurs at T_c. These three quantities are plotted versus concentration of V in Figures 2.5, 2.6, and 2.7, respectively.

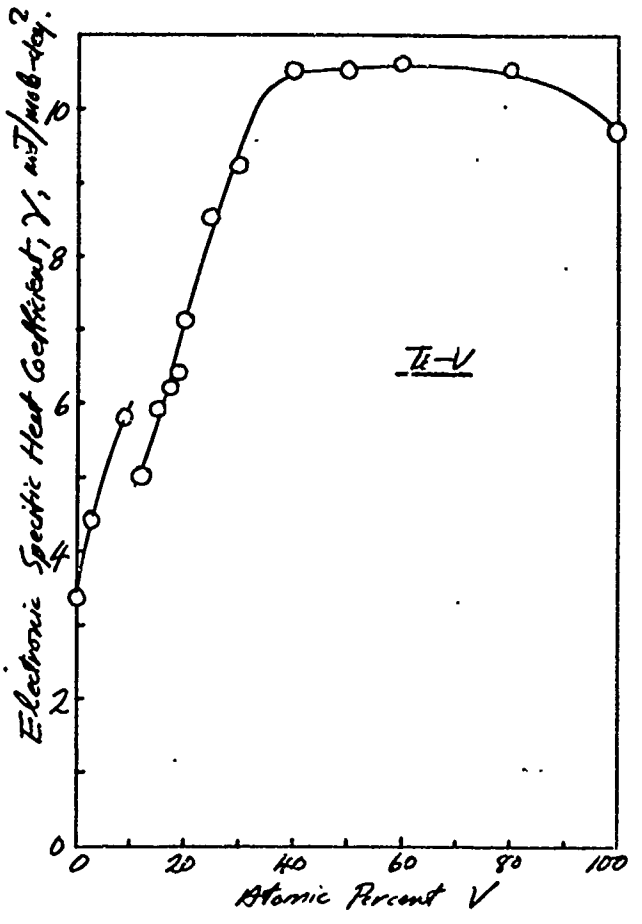

FIGURE 2.5. Composition-dependence of the electronic-specific-heat coefficient, γ, in Ti-V.

Particularly noteworthy is the similarity in shape between the γ and T_c curves; and the approximately inverse shape of the Θ_D profile (Figure 2.6).

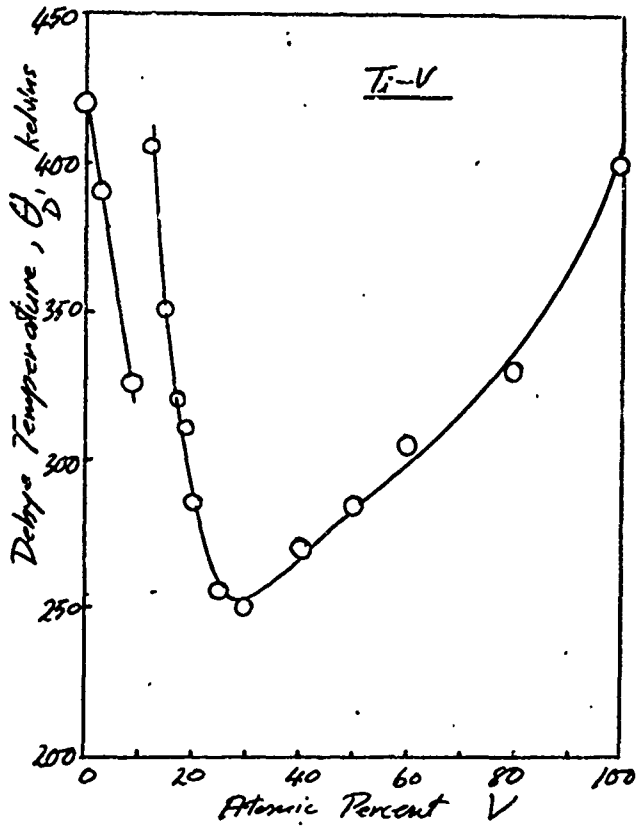

FIGURE 2.6. Composition-dependence of the Debye temperature, Θ_D, of Ti-V alloys.

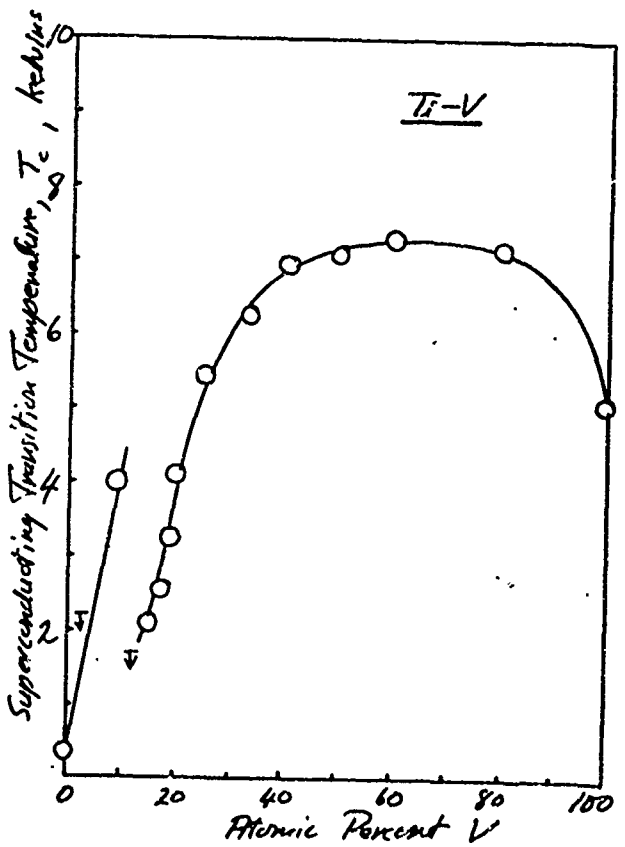

FIGURE 2.7. Composition-dependence of the superconducting critical temperature, T_c, in Ti-V alloys.

2.4. NMR Studies of the Ti-V System

One of the objectives in the first year of this program was to determine the feasibility of exploiting the microscopic character of NMR techniques to obtain direct, quantitative information about various properties, e.g. electronic structure and thermodynamic stability, of ω-phase precipitates in Ti-X alloys. In order to do this it is necessary to demonstrate that NMR signals from nuclei in the ω-phase precipitates are sufficiently well resolved from those in the background matrix to allow direct measurements on the ω-phase.

During the past year we have conducted an extensive investigation of the V^{51} NMR in a series of Ti-V alloys ranging in vanadium concentration from 6 to 90 atomic percent. Although the upper and lower regions of this concentration range are well outside the currently accepted limits for ω-phase precipitation in the Ti-V alloy system, it was necessary to study these regions in order to characterize the V^{51} resonance in the β and α phase, one or the other of which must always coexist with the ω-phase. Of course, the bulk of the NMR research was concerned with the 19 atomic percent vanadium alloy since it lies very near the center of the ω-phase precipitation region.

The NMR specimens were powders obtained by filing the arc melted samples. The powders were heat treated at 1000° C for 20 minutes to stabilize the β phase and subsequently quenched in ice brine. The V^{51} knight shift was measured as a function of vanadium concentration using conventional wideline techniques in conjunction with a signal averager. The results for a fixed operating frequency of 12 MHz are shown in Figure 2.8 along

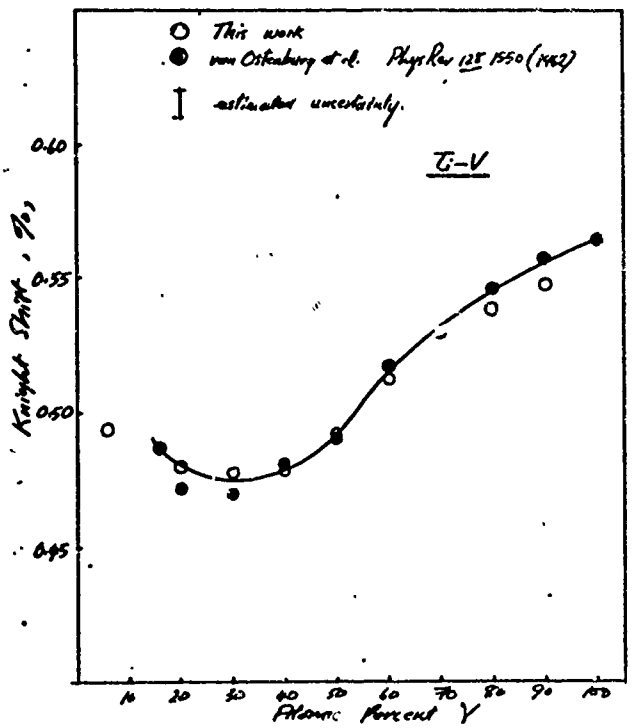

FIGURE 2.8. Composition-dependence of the knight shift in Ti-V.

with the knight shift data obtained by Van Ostenburg, et al. using specimens which were prepared under similar conditions. In discussing their results, Van Ostenburg et al., made no reference to field-dependent effects on the observed spectra or to the possible existence of ω-phase. In fact, they assumed that their specimens were homogeneous solid solutions and applied the rigid band model to relate the electronic structure to the concentration dependence of the knight shift; this implies that they did not find an appreciable field dependence of the lineshape or the knight shift. In contrast, we have observed that the resonance patterns show a pronounced field dependence, especially in the concentration range where ω-phase is believed to occur.

B. AGING STUDIES OF A Ti-V (19 at.%) ALLOY

The main thrust of the present program was the study of aging in a Ti-Nb or Ti-V alloy. Ti-V was selected as the more suitable since the NMR signal was more readily detectable. Compositions chosen for study were 15 at.% V and 19 at.% V. The aging characteristics of TV-19 have previously been investigated using conventional X-ray techniques (1).

2.5. Magnetic Susceptibility Studies of Aging in Ti-V (19 at.%)

Magnetic susceptibility measurements were carried out in several samples of TV-19. The specimens were initially given the standard quenching treatment, and were then aged at 300° C for various times of from 0.5 to 2,500 hours. The results are plotted semilogarithmically in Figure 2.9.

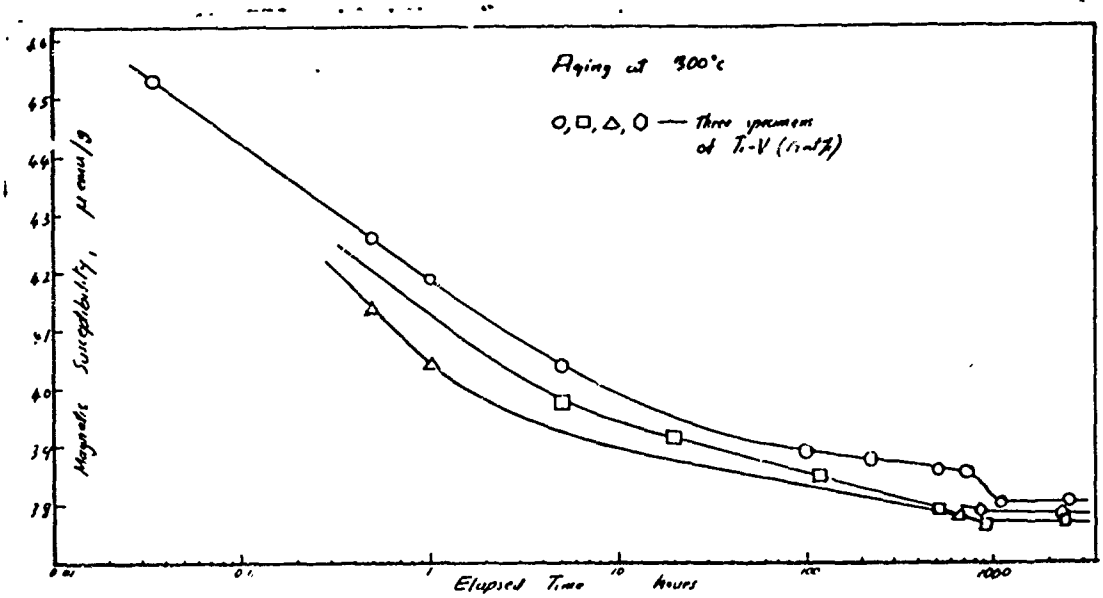

FIGURE 2.9. Influence of aging as the magnetic susceptibility, χ, of a Ti-V (19 at. %) alloy. Metastable (β+ω) equilibrium is achieved after about 800-1000 hours at 300° C.

The figure shows that magnetic susceptibility can be used as a sensitive indicator of the progress of the $\beta \rightarrow \beta+\omega$ aging process; and that in TV-19, aging can be regarded as having proceeded to "equilibrium" after about 800 to 1000 hours at 300° C.

2.6. Calorimetric Studies of Aging in TV-19

Low-temperature specific heat measurements were made on several specimens of TV-19, one of which was aged successively for 1, 5, 10, and 30 hours, while others were aged respectively for 100, 300, and 860 hours all at 300° C. A most interesting set of calorimetric data were obtained, as shown in Figure 2.10. Important points to be noted regarding the shapes of the specific-heat jumps in Figure 2.10 are:

(a) Aging for 1 hour at 300° C results in a slightly increased sharpness of the superconducting transition, compared to that for the as-quenched specimen, suggesting that some cooling strains may be present in the latter

(b) The curves representing aging for 100, 300, and 860 hour exhibit very broad superconducting transitions. It is very likely that at sufficiently low temperatures, the entire specimen becomes superconducting; but it seems as if a range of transition temperatures is involved. This effect will, of course, be examined further; and in analyzing the data we will attempt to associate a relatively short coherence distance with a wide spread of ω-phase particle diameters.

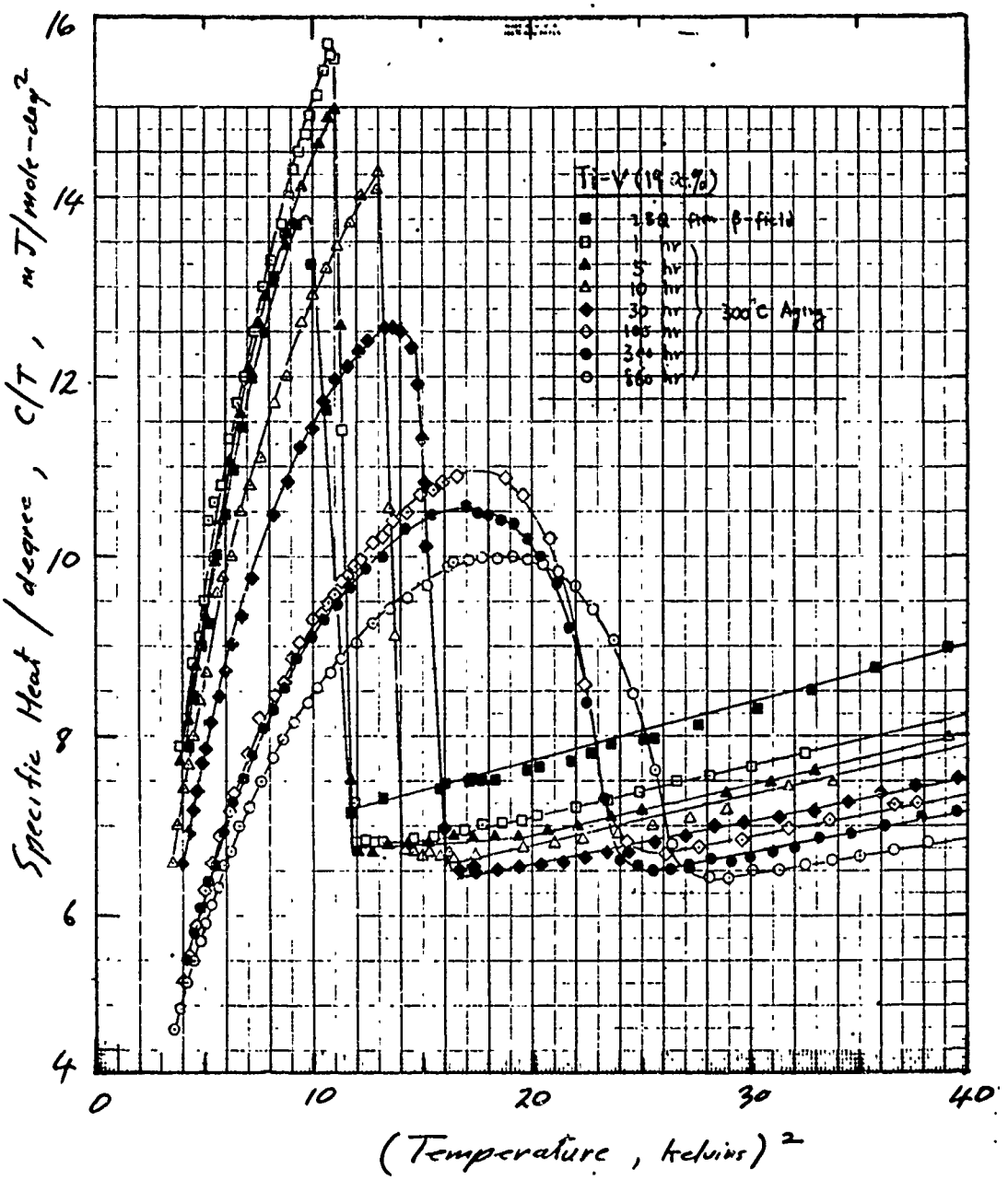

FIGURE 2.10. Response of the low-temperature specific heat of TV-19 to aging for various times between 1 and 860 hours at 300° C.

The influence of aging on γ and Θ_D is summarized in Table 2.5. Note that, because of the breadth of the superconducting transition, T_c is not included in this table.

TABLE 2.5. LOW-TEMPERATURE CALORIMETRIC PARAMETERS γ AND Θ_D AS FUNCTIONS OF AGING TIME AT 300° C IN A Ti-V (19 at.%) ALLOY

Aging Time Following Ice-Brine Quench, hours	γ, mJ/mole -deg^2	Θ_D, kelvins
0	6.40	310
1	5.95	325
5	5.75	325
10	5.65	325
30	5.60	345
100	5.45	345
300	5.30	350
860	5.30	370

2.7. NMR Studies of Aging in TV-19

For all vanadium concentrations above 6 atomic percent the V^{51} resonance linewidths increase monotonically with increasing magnetic field. Such behavior can only be explained by assuming a distribution of local fields at the vanadium sites due to one or more of the following situations:

(1) Local deviations in the vanadium concentration,

(2) Anisotropic knight shift effects due to local deviations from cubic symmetry,

(3) The presence of magnetic impurities, and

(4) Two, or more, different resonances associated with distinct phases in the alloy, e.g. β and ω.

In order to test the last possibility, we investigated the V^{51} resonance in the Ti-19% V alloy as a function of annealing time at 300° C. The results are shown in Figure 2.11. It is seen that the field dependent broadening mechanism is enhanced during the initial stages of the anneal, and that this enhancement becomes saturated before 299 hours. More significantly, the observed spectra, at least under the most favorable magnetic field conditions, showed evidence for the emergence of a partially resolved, second resonance as the annealing time was increased. Assuming that the V^{51} knight shifts in the ω and β phases are slightly different, the above qualitative results correlate extremely well with the expected growth of ω-phase during anneal at 300° C. However, since the different resonance peaks are only partially resolved, they cannot be studied independently, and it becomes necessary to compare the detailed shape of the observed resonance pattern with that predicted on a two resonance model. Although such comparisons are somewhat tenuous because of the many other broadening mechanisms which may exist in these alloys, it is believed that the model can be tested sufficiently well to determine its validity and that confirmation of the model will lead to important conclusions about the electronic structure and thermodynamic properties of ω-phase.

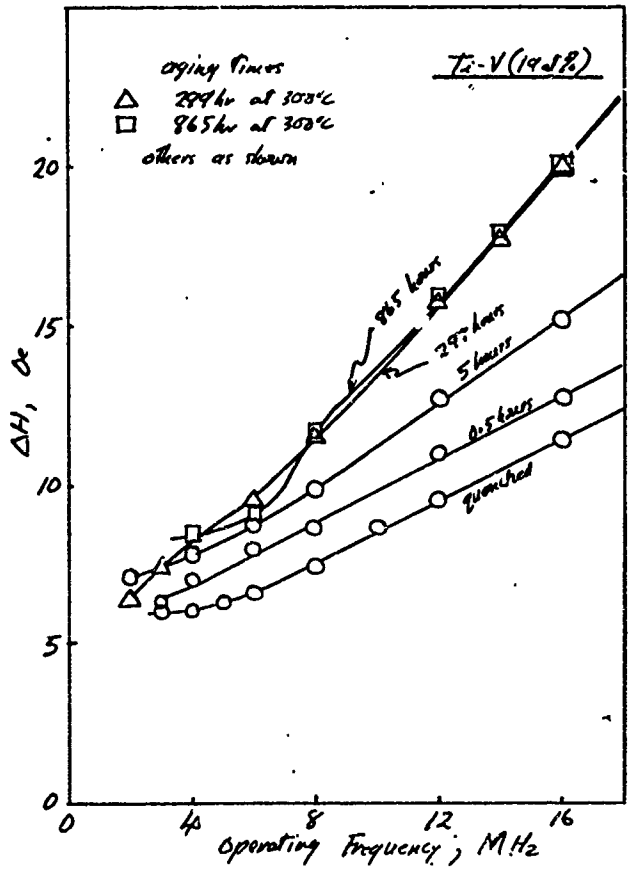

FIGURE 2.11. V^{51} NMR linewidth as a function of applied field in annealed Ti-V (19 at.%) alloys. (Note, the field is determined by the operating frequency divided by 11.246 MHz/10^4Oe.)

2.8. Conclusion

A reliable set of data on the electronic properties of the Ti-V alloy system has been obtained, and the effect of aging-to-saturation on these properties, with regard to TV-19, has been studied experimentally.

Work planned for the near future is an electron microscopic investigation of precipitation in TV-19. A series of aging experiments on TV-15 is also under way.

Data will eventually be analyzed in the manner described in Section 1, for Ti-Mo.

SECTION 3
MANUSCRIPTS PREPARED DURING THE YEAR

"Some relationships Between the Electronic and Mechanical Properties of Ti Alloys, Discussed From the Standpoint of Fundamental Alloy Theory", E. W. Collings, J. E. Enderby, H. L. Gegel, and J. C. Ho, Proceedings of the Second International Conference on Titanium, Boston, Mass., May 2-5, 1972.

"Interdependences of Electronic, Lattice-Vibrational, Elastic, and Microstructural Properties of Ti-Mo Alloys - I: Superconductivity and Electrical Resistivity of Ti-Mo", J. C. Ho and E. W. Collings (submitted to Second Int. Conf. on Titanium, Cambridge, Mass., May 2-5, 1972).

"Physics of Titanium Alloys - II: Fermi Density-of-States Properties and Phase Stability of Ti-Al and Ti-Mo", Proceedings of the Second International Conference on Titanium, Boston, Mass., May 2-5, 1972.

"The Inverse Scaling of the Low-Temperature-Specific-Heat Parameters γ and θ_D in Transition-Metal Binary Alloys and its Dependence on Phase Stability", E. W. Collings and J. C. Ho, submitted to Physics Letters.

SOME RELATIONSHIPS BETWEEN THE ELECTRONIC AND MECHANICAL PROPERITES OF Ti ALLOYS, DISCUSSED FROM THE STANDPOINT OF FUNDAMENTAL ALLOY THEORY

by

E. W. Collings, J. E. Enderby, H. L. Gegel,
and J. C. Ho

BATTELLE
Columbus Laboratories
Columbus, Ohio, USA, 43201

SOME RELATIONSHIPS BETWEEN THE ELECTRONIC AND MECHANICAL PROPERTIES OF Ti ALLOYS, DISCUSSED FROM THE STANDPOINT OF FUNDAMENTAL ALLOY THEORY*

E. W. Collings,† J. E. Enderby,†† H. L. Gegel,†††
and J. C. Ho††††

The results of two general theories, which when taken together enable the structure-dependence of the cohesive energy of an alloy to be related to the electronic structures (atomic and band) of the pure constituents, are applied in a discussion of solid solution strengthening in α-stabilized and β-stabilized Ti-base alloys.

* Supported by the Air Force Materials Laboratory, Wright-Patterson Air Force Base, Ohio, under Contract AF33(615)69-C-1594, and the U. S. Air Force Office of Scientific Research (AFSC) under Grant No. 71-2084.

† Battelle, Columbus Laboratories, Columbus, Ohio, 43201.

†† Department of Physics, University of Leicester, Leicester, England, LEI 7RH.

††† Air Force Materials Laboratory, WPAFB, Ohio, 45433.

†††† Department of physics, Wichita State University, Wichita, Kansas, 67208.

1. INTRODUCTION

The problem of finding some common ground between the metal physicist and the physical metallurgist has always been a difficult one, particularly when the electronic basis of mechanical strength in metals and alloys is under debate. Progress has been inhibited by, for example, the fact that some electronic properties of some materials are practically unaffected by mechanical deformation. Nevertheless, a proper description of a metal, as an assembly of positive ions in equilibrium with the conduction electrons, must eventually lead to an understanding of the principal interactions which control ionic motion during deformation. Accordingly we commence our discussion with an expression for the cohesive energy (E_{COH}) of a pure metal, expanded in terms of atomic potentials and structural arrangements. For an alloy, E_{COH} in this format may be regarded as being dependent on the atomic potential differences of the constituents, or some equivalent parameter. In applying this extension of the basic theory, particularly to alloys of transition metals with nontransition metals, we are guided by the results of Stern's[1,2,3] tight-binding theory of electronic structure.

Through the use of such concepts, *a postiori* qualitative explanations of various mechanical property trends in real metals (as distinct from perfect crystals) have begun to develop into useful alloy design criteria. The fundamental approach seems, at first inspection, to be applicable only to pure or single-phase materials, and as such, would be of only limited value. This difficulty can be overcome by applying the method separately to the individual components of a polyphase system. Since the particular mechanical behavior of interest in a given situation is usually dominated by the mechanical properties of only one of the component phases (e.g., brittle particles either precipitated uniformly or concentrated at grain boundaries), at least as much attention is paid to the intrinsic characteristics of such a phase as to those of the host alloy.

2. THE COHESIVE ENERGY OF METALS AND ALLOYS

2.1. Pure Metals

The cohesive, and hence the mechanical properties of metals and alloys, depend principally on the interaction of metallic ions with, and *via*, the conduction electrons. The cohesive energy is represented by E_{COH}, a component of the internal energy E, where:

$$E = E_{COH} + TS \; ; \qquad (1)$$

with S and T representing entropy and absolute temperature respectively. If constant volume conditions prevail, E_{COH} may be identified as the Helmholtz free energy.

The key statement in this approach to an understanding of electronic-property/mechanical-property interrelationships, takes the form of a series expansion of E_{COH} into components representing the contributions by (a) the electron gas itself, and (b) n-body (n = 1,2 ...) ionic interactions; thus:

$$E_{COH} = \sum_{i=1}^{n} E_i \ . \qquad (2)$$

Such an expression might well be used axiomatically[4], but has also been derived formally by Cohen[5] who pointed out how the free energy could in this way be resolved into structure-independent and structure-dependent components. The expansion for E_{COH} is dominated by E_1, which represents the contribution by the electron gas plus the self-energy of the ions imbedded in it. Being structure-independent it is this term which confers on metals and alloys their characteristic ductility. E_2 depends on pair-wise (central-force interactions, E_3 on triplet interactions, and so on. These are all structure-dependent, and therefore control the metal's resistance to deformation. The convergence of (2) depends on the strengths of the atomic potentials expressed in some suitable form.

For very weak potentials (such as pseudopotentials) the series may be terminated at n = 2[6]. Within the context of the topic under discussion such a truncated form of Equation (2) has been derived by Harrison[7] and by Blandin[8] using second-order perturbation theory. Under these conditions E_{COH} is only weakly structure-dependent. A second-order perturbation expression of E_{COH} is valid, for example, for the monovalent[9] pseudopotential metals Na and K, which are for this reason plastic at all temperatures.

If the atomic potentials are strong, perturbation theory may no longer be used and we return to the full expression for E_{COH}, entering the regime of interest to us here, in which third- and higher-order terms become significant. The resistance to deformation of a pure metal may thus be related to the strength of its atomic potential; one measure of which, as Cohen has suggested[5], being E_g/Δ, the ratio of a low-lying band gap to the width of the unperturbed energy band.

In this paper we employ these concepts, formerly applied in discussions of phase stability in metals and alloys, to gain a fundamental understanding of solid-solution strengthening in Ti-base alloys.

2.2. Alloys

As the above discussion indicates, strengthening in metals is accompanied by a breakdown of perturbation theory. This is the clue which leads to an understanding of solid-solution strengthening in alloys. As Stern(2) has pointed out, perturbation theory may be used in describing the electronic structures of alloys formed between two simple metals only if V_{12}/Δ is small, where V_{12} is the difference in the atomic potentials of the components. Thus V_{12} for an alloy plays the same role as E_g for a pure metal. By selecting solute elements whose potentials differ considerably from that of the host we can control the convergence of Equation (2) and consequently the degree of solid-solution strengthening.

When dealing with alloys, it may be more convenient to go directly to factors which govern the validity of perturbation theory, and hence which from this standpoint control the convergence of Equation (2) rather than to take the intermediate step of considering individual atomic potentials or their relative differences in the format V_{12}/Δ. This is because many alloys of interest are those formed between nontransition metals and transition metals. It is difficult to assign to a transition metal a meaningful "atomic potential", particularly one that would be valid in a mixed alloy. On the other hand it is more straightforward to consider directly, and perhaps in a more fundamental way, the strong perturbation of electron states that result when a nontransition metal is alloyed with a transition metal.

3. ELECTRONIC STRUCTURES OF ALLOYS

The atoms of a pure simple metal (metal 1) of valence Z each contribute Z electrons to the conduction band. Similarly for a pure simple metal (metal 2) of valence Z + 1. But this is no longer true when metal 2 is dissolved in metal 1; since screening or charge-neutrality considerations require the extra valence electron to be more-or-less localized in the vicinity of the metal-2 atoms. This example, discussed initially by Mott(10) and developed into theories of metallic virtual bound states by Friedel(11) and into the theory of "charging", through the work of Stern(1,2,3), shows clearly that the perturbation approach and the rigid-band model are inapplicable to alloys of simple metals differing in valence. The theory of charging implies more than just a cell-by-cell neutralization of net charge by screening. If charging is "large"(1) the theory requires in addition a drastic alteration in band shape as the electrons are redistributed in energy. Thus, for example, the screening electrons of atom 1 may be assigned mostly to low-lying states in the band, and conversely for atom 2. Such an arrangement would imply the existence of a minimum in the n(E) (density-of-states *versus* energy) curve. In contrast to the motion of "neutral pseudo-atoms"(12) which carry their "own" screening electrons with them, the movements of atoms

under conditions of large charging are resisted by the energy barriers associated with redistribution of the screening charge in space and energy with each change of local environment. This strong structure-dependence of electron states which accompanies large charging is expressive of solid-solution strengthening.

Three results from the above theory, particularly important in this context are summarized below.

3.1. Transition-Metal Binary Alloys (T_1-T_2 Alloys)

Charging is particularly small in alloys between adjacent transition elements near the middle of a long period[3,13]. Excellent agreement with the rigid-band model has in fact been demonstrated by McMillan[14] for adjacent binary alloys from the sequence Hf-Ta-W-Re. We would not expect to find such good adherence to rigid-band principles for Ti-rich alloys with nearby transition elements, but nevertheless such alloys may still be classed as "low perturbation".

3.2. Transition-Metal/Nontransition-Metal Binary Alloys (T_1-B Alloys)

For isolated transition-metal ions dissolved in simple metals, the amplitudes of the d wavefunctions are large in the vicinity of the impurity. These are referred to as virtual bound states[11]. Together with some extra broadening of the d-states this picture carries over to concentrated alloys, with the result that we again find maximal d-wave-function amplitudes at the transition-metal-ion sites. The tendency of the d wavefunctions to stay away from the nontransition-metal sites leads to an approximate representation of the alloy as a "diluted" or "expanded" transition metal lattice. This model is substantiated by several pieces of experimental evidence. For example, as a result of NMR studies of the V-Al system, Van Ostenburg, et al[15], were able to demonstrate that the d-band electrons tended to avoid the Al cells. It is useful to interpret this as strong scattering of the d wavefunctions by the Al ions. In addition, the above authors were able to conclude that the valence electrons of the Al appeared to contribute to a low-lying band; a suggestion which later appeared[1] as a part of Stern's tight-binding theory of disordered alloys. Although somewhat more refined, the conclusions reached by Lye[16] with regard to the electronic structures of intermetallic components of Ti with the nonmetallic "p-s" elements C, N, and O, based on the results of band-structure calculations for TiC, are also in general agreement with these ideas.

For a T_1-B alloy, therefore, the picture which emerges is one of strong noncentral interactions between the ions, resulting in a pronounced structure-dependence of the corresponding E_{COH}.

3.3. Influence of Order-Disorder on Electron States

Stern's theory[1] shows that in the presence of small charging an electron energy band splits into two when the alloy orders. On the other hand, when $V_{12}/\Delta >> 1$ the model yields a band gap in both the disordered and ordered states of the alloy. The real situation will presumably be less well defined than this; nevertheless, as some of us have pointed out elsewhere[4], it is clear that various degrees of electronic structure change can be expected to accompany order-disorder. It can be argued that in general (there is at least one exception) the disordered alloy will tend to be the more ductile.

4. APPLICATION TO ALLOYS OF TITANIUM

4.1. Alloys of Ti With a Nearby Transition Metal (Ti-T_2 Alloys)

As indicated in 3.1., Ti-base transition-metal-binary (Ti-T_2) alloys may be classified as "low-perturbation". If T_2 is close to Ti in the transition-metal block of the periodic table, many of the properties of Ti-T_2 alloys are determined by the average electron-to-atom ratio, z. For example, when z exceeds a threshold value of about 4.4 the bcc (β) structure remains stable during quenching. We Therefore regard T_2 solutes as structural (β) stabilizers rather than solid-solution strengtheners, although some degree of strengthening may be contributed by their presence. Having obtained a suitable β-stabilized binary alloy, a second solute species may then be selected solely on the basis of its strengthening properties. This will generally be a nontransition element.

4.2. Alloys of Ti With Nontransition Metals -- Low-Concentration Ti-B Alloys

Significant solid-solution strengthening is achieved by adding nontransition metals (designated B-metals) to Ti. As indicated in 3.2., Ti-B alloys are characterized by a relatively high density of occupied d-states at the Fermi level. The d-wavefunctions are strongly scattered from the B-ions, which are themselves screened by electrons occupying states in the lower part of the band. During alloying, as the Ti-lattice becomes diluted or "expands", the influence on the Fermi density-of-states, $n(E_F)$, of a decreasing d-band width tends to be compensated for by a decrease in the average volume-density of d-states. The resultant relatively small concentration-dependence of $n(E_F)$ with alloying, in low-concentration Ti-Al alloys, has already been demonstrated[17].

It is possible to enumerate several important consequences of the rearrangement of electron states which accompanies the addition of B-metals to Ti.

4.2.1. The Cohesive Energy

Of primary concern to us here is the fact that the readjustment of the energy state of B which accompanies its solution in Ti can be designated as a "strong interaction" between B and its Ti neighbors. The increase in structure-dependence of E_{COH} through the necessity of including high-order terms in Equation(2) is an expression of solid-solution strengthening. Listed below are some of the various physical property measurement techniques which may be employed in studying the magnitude of this interaction strength.

4.2.1(a) Relative Vapor Pressure. The application of this technique in the determination of thermodynamic activities and pair-wise interaction parameters is discussed elsewhere in these proceedings(18).

4.2.1(b) The Electrical Resistivity. As pointed out above, it is possible to relate the solid-solution-strengthening capacity of B, when dissolved in Ti, to the scattering potential presented by B-ions to d-wavefunctions. Thus the relative magnitudes of the specific resistivities(19) of various metals when dissolved in Ti, can be used as indicators of the degrees of charging, and consequently of solid-solution strengthening. The composition-dependences of resistivity of several Ti-T_2 and Ti-B alloys are shown in Figure 1. It is seen immediately that the specific resistivity common to various T_2 ions in Ti is about an order of magnitude smaller than those for B-metals; a result consistent with Sections 4.1 and 4.2. Furthermore the resistivity data suggest that the interaction strengths between various B-metals and Ti, and hence the solid-solution-strengthening abilities of the B-metals in Ti-B alloys, increase in the sequence Al → Ga → Sn. This has indeed proved to be the case for Al and Ga additions to Ti, as indicated in Figure 2.

4.2.2. Phase Stability

In contrast to transition-metal solutes, additions of which increase the d-electron density and lead eventually to β-stabilization; the "p-s" elements (particularly the B-metals) by "diluting" the Ti lattice in the manner outlined in Section 3.2, yield solid solutions which remain "Ti-like" as alloying proceeds. This is the mechanism of α-stabilization.

In other papers(20) we have usually defined an electron-to-atom ratio ($\bar{z}$) scale by considering the average number of valence electrons (i.e., the atomic d, s electrons for Ti; and the p, s electrons

for Al). However, the dilution concept referred to above, together with the conclusions of other workers[21], suggest that a more physically meaningful $\bar{z}$-type scale, valid for both Ti-T_2 and Ti-B alloys, might result if we restricted ourselves to a consideration of the average density of only the d-electrons.

4.2.3 Ternary Solid-Solution Strengthening

For a given total solute concentration we would generally expect to observe an improvement in solid-solution strengthening in going from a binary to a ternary (Ti-B_1-B_2) alloy, as the binary Ti-B_i-type interactions become augmented by interactions (B_1-B_2) between the solute atoms themselves. An example of this is given in Figure 2 which illustrates a "secondary" solid-solution strengthening of Ti-Ga accompanying the substitution of Al for half of the Ga formerly present. In that figure it is interesting to note that the Ti-xAl-xGa curve lies above that for Ti-Ga, rather than between those for Ti-Al and Ti-Ga as might otherwise have been expected. Numerical values of the pair-wise interaction parameters appropriate to the Ti-Al, Ti-Ga, and Al-Ga interactions respectively, are presented elsewhere in these proceedings[18].

Finally we note that these principles of solid-solution strengthening can be extended to β-stabilized (i.e., Ti-T_2) alloys, which may thus be strengthened through additions of the elements B_1, B_2, etc.

4.3. Alloys of Ti With Nontransition Metals -- High-Concentration Ti-B Alloys

The strong spacial correlations which characterize the structures of Ti-B alloys lead eventually, as the alloys become more concentrated, and hence as the atom-ratio n_{Ti}/n_B becomes smaller, to long-range-ordered sturcutres. A good example of this effect is to be found in the Ti-Al system. At, say, 700° C Ti-Al alloys with Al concentrations of 21 through 25 at.% assume the long-range-ordered α_2 structure[22]. The influences of such ordering on the electronic transport and density-of-states properties of Ti-Al are described elsewhere[4,17,23], the experimental results being consistent with a considerable reduction of $n(E_F)$ with ordering, particularly in Ti_3Al.

4.3.1 Influence of Order-Disorder on Electronic Structure and Mechanical Characteristics

Referring to previous sections (the above, and Section 3.3) and elsewhere[4] the results of both theory and experiment indicate that changes in electronic structure are expected to accompany order-disorder in most alloys except those characterized by small value of

the parameter V_{12}/Δ. For example, in Ti_3Al the ordered α_2 structure supports, and is supported by, a significant degree of bond directionality(23,24).

It follows that deformation of a long-range-ordered structure results in a reduction in the order-parameter, and consequently a change in the electronic structure. This is not necessarily true for a disordered alloy, deformation of which merely results in another disordered structure. As a result, an ordered alloy tends to resist deformation to a greater extent than it otherwise would, if in the disordered state(25). A classical exception to this is Mg_3Cd(26) whose deformation properties require individual treatment.

Thus it is generally possible to alleviate the brittleness associated with a given intermetallic compound by destroying the long-range order. Two methods of disordering, or partially disordering, binary compounds are available: (a) isothermal disordering through the addition of a third atomic species; (b) thermal disordering by heating through the order-disorder critical temperature, T_c. Examples of these are as follows.

4.3.1.(a). A significant reduction in the brittleness associated with Ti_3Al is achieved by the substitution of Ga for some of the Al, within the "ordered" lattice. This procedure also results in a reduction in T_c from 850° C for Ti_3Al to 640° C for "$Ti_3Al_{1/2}Ga_{1/2}$".

4.3.1.(b). Disordering can be achieved thermally by heating through T_c. At the same time we would expect to find an improvement in ductility. That this does indeed take place in "$Ti_3Al_{1/2}Ga_{1/2}$" is evidenced by Figures 3(a) and (b) which show a correlation between the order-disorder and brittle-ductile transformation temperatures. Microscopically, we have interpreted this behavior in terms of a relatively high structure-dependence of E_{COH} in the ordered phase. Thermodynamically, in considering the effect of temperature, and ultimately disordering, on ductility we return to Equation (1). For $T > 0$, E_{COH} is augmented by the "structure-independent" term TS which normally increases smoothly with temperature; but which in addition undergoes a relatively large rapid increase as T approaches T_c.

5. SUMMARY

The resistance to deformation of a metal is gauged by the extent to which the cohesive energy, E_{COH}, is structure-dependent. E_{COH} may be expanded in the form:

$$E_{COH} = \sum_{i=1}^{n} E_i \qquad (1)$$

in which E_n represents n-body interactions. The convergence of (1) is controlled by the strengths of the atomic potentials, in the case of pure metals; or the atomic potential differences between the constituents, in the case of alloys— in other words by the extent to which perturbation theory is valid. These principles have been employed to provide a fundamental understanding of phase stability and solid-solution strengthening in Ti-base alloys.

(a) When alloyed with B-metals the lattice remains "Ti-like" and consequently α-stable. The alloying of Ti with other transition elements β-stabilizes the lattice when the electron-to-atom ratio ($\bar{z}$) becomes suitably large ($\bar{z} \gtrsim 4.4$).

(b) Solid-solution strengthening may be achieved by adding B-metals either to Ti, resulting in strengthened α-alloys; or to Ti-T_2 ($\bar{z} \gtrsim 4.4$) alloys, to produce strengthened β-alloys.

(c) "Secondary" solid-solution strengthening through B_1-B_2-type interactions may be achieved through the use of several B-metal additions to form Ti-B_1-B_2-etc. α-alloys, or Ti-T_2-B_1-B_2-etc. β-alloys.

(d) The embrittlement associated with "excessive" solid-solution strengthening of binary α-alloys to the point of ordered compound (e.g. α_2) formation may be alleviated by disordering, accomplished either through ternary alloying or thermally.

REFERENCES

1. E. A. Stern, Physics, 1, 255 (1965).

2. E. A. Stern, Phys. Rev., 144, 545 (1966).

3. E. A. Stern in "Energy Bands in Metals and Alloys", ed. by L. H. Bennett and J. T. Waber, Gordon and Breach (1968), p 151.

4. E. W. Collings, J. E. Enderby, and J. C. Ho in Proceedings of the 3rd Materials Research Symposium "Electronic Density of States", Nat. Bur. Stand. (U.S.) Spec. Publ. 323, Dec. 1971, p 483.

5. M. H. Cohen in "Alloying Behavior and Effects in Concentrated Solid Solutions", ed. by T. B. Massalski, Gordon and Breach (1965), p 1.

6. M. H. Cohen in Colloquium on Solid Metallic Solutions, Orsay, 1972, J. Phys. Radium, 23, 643 (1962).

7. W. A. Harrison, "Pseudopotentials in the Theory of Metals", Benjamin (1966).

8. A. Blandin in "Alloying Behavior and Effects in Concentrated Solid Solutions", ed. by T. B. Massalski, Gordon and Breach (1965), p 50; see also R. Pick and A. Blandin, Phys. kondens. Materie, 3, 1 (1964).

9. The situation becomes more complicated with polyvalent metals, because of the interrelationship between structure and band structure as discussed by V. Heine in "Phase Stability in Metals and Alloys", ed. by P. S. Rudman et al., McGraw-Hill (1967), p 103.

10. N. F. Mott and H. Jones, "The Theory of the Properties of Metals and Alloys" (1936), Dover Publications (1958), p 86.

11. J. Friedel, Advances in Physics, 3, 446 (1954) [e.g., p 477]; see also numerous subsequent papers, e.g., J. Friedel in "Proceedings of the International Conference on Electronic Transport in Metals and Solids (1956); Can. J. Phys., 34, 1190 (1956).

12. J. M. Ziman, Advances in Physics, 13, 89 (1964).

13. J. Friedel, discussion in "Phase Stability in Metals and Alloys", ed. by P. S. Rudman, et al., McGraw-Hill (1967), p 162.

14. W. L. McMillan, Phys. Rev., 167, 331 (1968).

15. D. O. Van Ostenburg, et al., Phys. Rev., 135, A455 (1964).

16. R. G. Lye in "Atomic and Electronic Structure of Metals", ed. by J. J. Gilman and W. A. Tiller, Chapman and Hall (1967), p 99.

17. E. W. Collings and J. C. Ho in "The Science, Technology, and Application of Titanium", Proceedings of an International Conference, 1968, ed. by R. I. Jaffee and N. E. Promisel, Pergamon Press Ltd. (1970), p 331.

18. H. L. Gegel and M. Hoch, "Thermodynamics of α-Stabilized Ti-X-Y Systems" -- paper 11 of this Session.

19. Specific resistivity is defined as the increment in resistivity per at.% solute.

20. See for example papers 2 and 3 of this Session.

21. E. S. Fisher and D. Dever, Acta Met., 18, 265 (1970).

22. M. J. Blackburn, Trans. AIME, 239, 1200 (1967).

23. J. C. Ho, P. C. Gehlen, and E. W. Collings, Solid State Comm., 7, 511 (1969).

24. P. C. Gehlen in "The Science, Technology, and Application of Titanium", Proceedings of an International Conference, 1968, ed. by R. I. Jaffee and N. E. Promisel, Pergamon Press Ltd. (1970), p 349.

25. N. S. Stoloff in "Fracture", ed. by H. Liebowitz, Academic Press (1969), pp 2-77 (in particular p 53).

26. N. S. Stoloff and R. G. Davies, Trans. ASM, 57, 247 (1964).

LIST OF FIGURES

Figure 1. Composition dependences of resistivity for Ti-T_2 and Ti-B alloys. The data for Ti-T_2 alloys are from S. L. Ames and A. D. McQuillan Acta. Met. 4 619 (1956). The results show that the interaction strengths of various solute elements with Ti proceed in the sequence T_2, Al, Ga, Sn.

Figure 2. The solid-solution strengthening capacities of B-metals dissolved in Ti increase in the sequence Al, Ga, in agreement with the data of Figure 1. In addition it can be seen that "secondary" solid-solution strengthening results in a ternary alloy (Ti-Al-Ga) which is stronger than Ti-Ga.

Figure 3. (a) Magnetic determination of the order-disorder critical temperature, T_c, in "$Ti_3 Al_{1/2} Ga_{1/2}$". (b) Increase in ductility in "$Ti_3 Al_{1/2} Ga_{1/2}$" on approaching T_c.

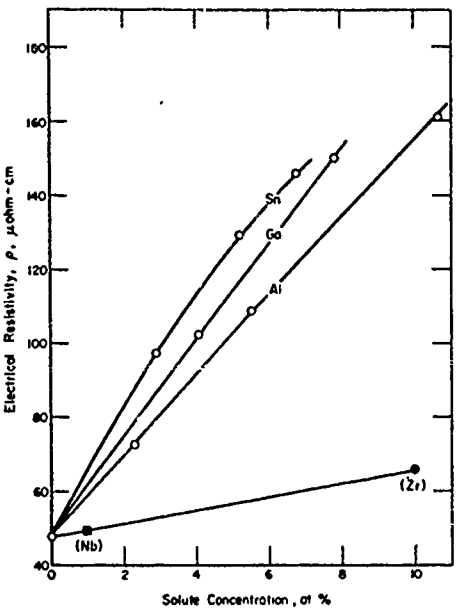

Figure 1. Composition dependences of resistivity for Ti-T_2 and Ti-B alloys. The data for Ti-T_2 alloys are from S. L. Ames and A. D. McQuillan Acta. Met. 4 619 (1956). The results show that the interaction strengths of various solute elements with Ti proceed in the sequence T_2, Al, Ga, Sn.

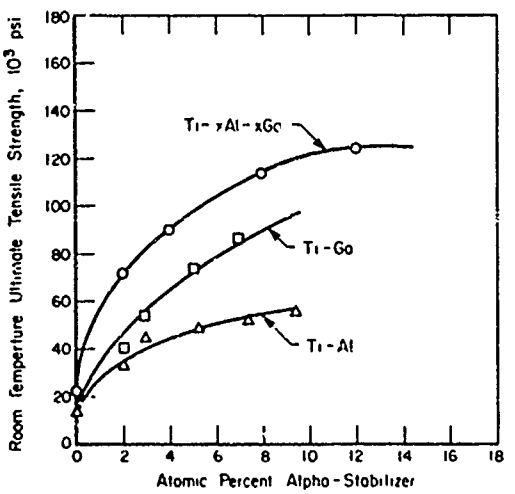

Figure 2. The solid-solution strengthening capacities of B-metals dissolved in Ti increase in the sequence Al, Ga, in agreement with the data of Figure 1. In addition it can be seen that "secondary" solid-solution strengthening results in a ternary alloy (Ti-Al-Ga) which is stronger than Ti-Ga.

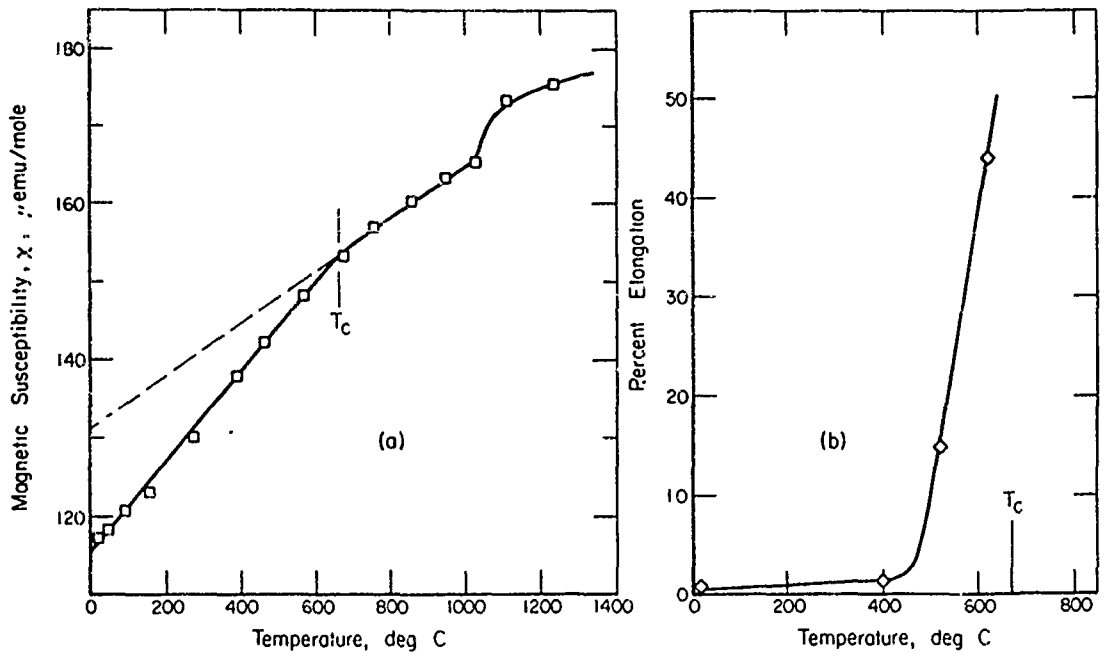

Figure 3. (a) Magnetic determination of the order-disorder critical temperature, T_c, in "$Ti_3 Al_{1/2} Ga_{1/2}$". (b) Increase in ductility in "$Ti_3 Al_{1/2} Ga_{1/2}$" on approaching T_c.

PHYSICS OF TITANIUM ALLOYS-I: ALLOYING AND MICROSTRUCTURAL EFFECTS IN THE SUPERCONDUCTIVITY OF Ti-Mo

by

J. C. Ho and E. W. Collings

BATTELLE
Columbus Laboratories
Columbus, Ohio, USA, 43201

PHYSICS OF TITANIUM ALLOYS*-I: ALLOYING AND MICROSTRUCTURAL EFFECTS IN THE SUPERCONDUCTIVITY OF Ti-Mo

J. C. Ho† and E. W. Collings
BATTELLE
Columbus Laboratories
Columbus, Ohio 43201

In this, the first of a pair of papers reviewing some of the physical properties of Ti alloys, the conjoint influences of solute concentration and microstructural state on the superconducting transition temperature of Ti-Mo are discussed.

In a series of ice-brine-quenched Ti-Mo alloys whose structures are successively α' (0 to ~4-1/2 at.% Mo), β+ω (5 to ~15 at.% Mo), and β (≳15 at.% Mo) the superconducting transition temperature, T_c, first increases rather rapidly with increasing Mo concentration [Mo]; taking on enhanced values within the α' regime through the operation of a mechanism based on a high density of suitably "soft" vibrational states, a property of the α' structure. But immediately upon entering the (β+ω) field, T_c drops to a very low value due to the depressant influence of a high density of ω-phase precipitates. T_c then increases again with increasing [Mo] as the volume fraction of ω-phase precipitation decreases. At higher concentrations (≳20 at.%) T_c decreases with increasing [Mo], an effect which we deduce to be characteristic of single-phase-bcc transition-metal binary alloys within the electron-to-atom-ratio ($\bar{z}$) range from 4 to 6.

*Supported by the Air Force Materials Laboratory, Wright-Patterson Air Force Base, Ohio, under Contract AF33(615)69-C-1594, and the U.S. Air Force Office of Scientific Research (AFSC) under Grant No. 71-2084.

†Present address: Department of Physics, Wichita State University, Wichita, Kansas, 67208.

1. INTRODUCTIO

The results of some low-temperature specific heat and magnetic susceptibility measurements on a pair of representative Ti alloy systems: α-stabilized Ti-Al, and β-stabilized Ti-Mo, were presented and discussed at the First International Conference on Titanium (London, 1968)[1]. In this and a companion paper (henceforth II), in which some of the subsequent developments of that work are reviewed, and some new results are outlined, the interdependences of various electronic and microstructural properties are emphasized.

The superconducting properties of a sequence of Ti-Mo alloys (designated TM-x, where x is the Mo concentration in at.%) were studied using low-temperature calorimetry as principal experimental technique. Interpretation of the specific-heat data was aided by magnetic-susceptibility investigations; and also by optical- and electron-microscopic studies of the as-quenched and aged microstructures. Figures 1 and 2 can be regarded as summarizing the joint compositional and microstructural dependences of the superconducting transition temperatures (T_c) of the quenched Ti-Mo alloys. As indicated by the nonequilibrium diagram of Figure 1 (b), the 30-40g specific-heat ingots of Ti-Mo after ice-brine quenching from 1300° C, exhibited structures which were thermal martensitic (α') up to 4-1/2 at.% Mo and basically bcc at higher compositions. However, according to the literature[2,3,4] and our own electron microscopic studies[1,5] quenched ingots of compositions through 10 at.% Mo, and possibly as high as 15 at.% support ω-phase precipitation [Figure 2(a)]. As is well known by now the ω-phase is submicroscopic in size[6] and hexagonal in crystal symmetry. The equilibrium and nonequilibrium structures indicated in Figures 1(a) and 1(b) represent extreme states of the Ti-Mo system between which many different structural states may exist depending on both mechanical and thermal treatments.

Figure 2(b), which shows that T_c depends strongly on the structural state as well as the alloy composition, serves to introduce the following discussion dealing with the influences on T_c of (i) thermal and deformation martensites (α' and α" respectively) and (ii) controlled ω-phase precipitation.

2. THERMAL AND DEFORMATION MARTENSITES

Figure 2(a) indicates that in quenched Ti-Mo the α' region terminates fairly abruptly within a narrow composition range near 4-1/2 at.% Mo while Figure 2(b) shows T_c to increase rapidly, at the rate of about 1 degree per at.% Mo, within that regime. A comparison of curves (b) and (d) in Figure 2 showed that the relative rate of increase of T_c with composition was significantly greater than the corresponding relative rate of increase to electronic-specific-heat coefficient, γ [a measure of the Fermi density-of-states, $n(E_F)$[7]],

suggesting that some kind of T_c enhancement mechanism was operative.[8] Anomalies in the expected relationship between T_c and γ can best be expressed with the aid of a BCS-Morel-Morin-Maita[9] plot of log (T_c/Θ_D) versus $(0.212\ \gamma)^{-1}$, where Θ_D is the calorimetrically-measured Debye temperature. Presented in this way (Figure 3) the data clearly show that α' alloys are characterized by almost threefold enhancements of T_c in comparison with values expected for the same materials were they to possess nonmartensitic [i.e. β or $(\beta+\omega)$] structures. An enhanced T_c is a quite general characteristic of α' Ti-T_2 and Zr-T_2 alloys (where T_2 represents another transition element)[10]. This is exemplified by Figure 4 in which the T_c-composition-dependence of Ti-Mo and Ti-Fe are compared. That figure also implies that it is no longer necessary to invoke a "magnetic" electronic interaction of the type previously suggested[11,12,13], in order to explain the enhanced transition temperatures, first thought to be properties only of dilute alloys of Ti with "magnetic" transition element solutes.

A detailed study was made of superconductivity in TM-4-1/2, whose composition placed it at the terminus of the quenched α' regime[14]. The results of that work, together with the known close relationship between thermal (α') and deformation (α'') martensites suggested that it might be possible to induce enhanced values of T_c in low-concentration $(\beta+\omega)$-Ti-Mo alloys by subjecting them to mechanical deformation of sufficient severity. Alloys of 5 and 7 at.% Mo were chosen for further experimentation[15]. The results of low temperature specific heat measurements on TM-5, for example, taken before and after compressive deformation are summarized in Figure 5[15,16]. In the quenched state $(\beta+\omega)$ the transition temperature, which was below the lower temperature limit of the apparatus, was estimated to be about 1 K based on Figure 3 and the measured γ and Θ_D values. After being deformed at room temperature, during which α'' was induced, the same specimen yielded a threshold T_c of 3.3 K. Figure 3 indicates the transition temperatures of TM (5 and 7) as special points (Δ) falling near those for alloys possessing the α' structure. For α' and α'' alloys, it is not possible to attribute these enhanced T_c's to electronic-density-of-states effects within the framework of the BCS-theory using the interaction parameter, derived from the slope of the line in Figure 3, which was common to all the nonmartensitic alloys. Instead we conclude that the enhanced transition temperatures occur as a result of the extreme lattice distortion or disorder, which is responsible for increased electron-phonon-electron coupling in the manner described by McMillan[17], and Garland et al.[18].

3. ω-PHASE PRECIPITATES

3.1 Composition-Dependence of T_c in As-Quenched Ti-Mo Alloys

Returning to Figure 2(b) we see that after rising to a relatively high value at the terminus of the martensitic (α' and α'') regime, T_c drops below the lower temperature limit ($\sim$1.5 K) of our calorimeter as the quenched microstructure changes to ($\beta+\omega$). T_c then increases again with solute concentration, and passes through a maximum at an electron-to-atom ratio ($\mathcal{Z}$) near 4.4. A set of low-temperature specific heat data for the alloys TM-5 through 15 is included for reference as Figure 6. Particularly noticable are the small widths ($\sim$0.15 degrees) of the superconducting transitions. Moreover the relative heights of the specific-heat jumps at T_c, i.e. $[\Delta C/T_c)/\gamma]$, are sufficiently close to the BCS-prescribed value (viz. 1.43) as to be indicative of bulk transitions. The sharpness and homogeneity of the calorimetrically measured superconducting transitions for alloys in the range $4.1 \lesssim \mathcal{Z} \lesssim 4.3$ were misinterpreted by earlier workers, who believed that such alloys were single-phase bcc (β); and consequently that the maximum in T_c was the result of a maximum in $n(E_F)$ which was thus assumed to be characteristic of β-phase alloys at $\mathcal{Z} \cong 4.3$ or 4.4. However, the existence of ω-phase precipitation in representative alloys (e.g. TM-5 and 10) within $4.1 \lesssim \mathcal{Z} \lesssim 4.3$ was suspected[2,3,4] and eventually established by direct observation[1,5]. Accordingly, it was reasonable to postulate[19] that the maximum in T_c was <u>induced</u> in an otherwise monotonic function of T_c <u>versus</u> $\mathcal{Z}$ by a proximity-effect-induced depression of T_c brought about by the presence of the ω-phase. If this were true then it should be possible (a) to increase T_c by removal of the ω-phase; and (b) to bring about further depression in T_c by encouraging the ω-phase to develop. The results of this pair of tests of the initial postulate are outlined below.

3.2 Composition-Dependence of T_c in Hypothetical ("Unstable") Single-Phase bcc (β) Ti-Mo, $0 \lesssim \mathcal{Z} \lesssim 4.3$

To establish references, against which to compare the physical properties of ω-phase-containing alloys, and eventually ω-phase itself, we set out to make estimates of γ, χ, and T_c for hypothetical ["unstable"[20]] β-Ti-Mo in the temperature regime for which $\mathcal{Z} \lesssim 4.3$. These were based on the extrapolated results of magnetic-susceptibility-temperature-dependence, $\chi(T)$, studies carried out in the elevated-temperature equilibrium-β field, as indicated by the dashed line of Figure 2(c). After observing the manner in which the composition dependences of χ, γ,[5] (and T_c), for the as-quenched alloys tended to scale [c.f. the full lines of Figures 2(c), (d), (and (b)), respectively], we were reasonably confident in using the extrapolated magnetic data to deduce the composition-dependence of

γ(β-Ti-Mo) within $0 \lesssim \mathcal{Z} \lesssim 4.3$. The result is indicated by the dashed line of Figure 2(d). The γ's so obtained were then applied to a short extrapolation of the log (T_c/Θ_D) versus $1/(0.212\ \gamma)$ plot of Figure 3, in order to derive a set of (T_c/Θ_D)-values for unstable Ti-Mo. Calling once more on the χ, γ, T_c scaling relationship, separate sets of values of T_c and Θ_D were then extracted, using smoothness as one criterion. That is to say, following the behavior χ(β-Ti-Mo, 300 K), which was found to increase monotonically as $\mathcal{Z}$ decreased from 6.0 to 4.0 rather than to pass through a maximum at $\mathcal{Z} \approx 4.3$, T_c was extrapolated back into the unstable regime, increasing as $\mathcal{Z}$ decreased, as a smooth continuation of the directly measured stable-β locus [dashed line in Figure 2(b)]. At the same time the coupled quantity, Θ_D, dropped rather rapidly as $\mathcal{Z}$ decreased below 4.3. This is a physically realistic result, in that it expresses a continuous softening of the unstable β lattice as the condition for "absolute instability" [viz. $(c_{11}-c_{12}) \leq 0$ for $\mathcal{Z} \lesssim 4.1$] is approached.

Table I. Superconducting-Transition, And Debye Temperatures [T_c, Θ_D, respectively], And Fermi Density-of-States [$n(E_F)$], in Ti-Mo Alloys

Alloy Designation		T_c (kelvins)		Θ_D (kelvins)		$n(E_F)$ States/eV-Atom	
		β	β+ω	β	β+ω	β	β+ω
Pure Ti	4.00	[6.4]	--	[200]	--	[1.50]	--
TM-5	4.10	5.0_5	<1.5	207	380	1.35	0.75
TM-7	4.14	4.8_0	2.1	220	350	1.30	0.89
TM-8-1/2	4.17	4.5_9	2.8	232	320	1.25	0.97
TM-10	4.20	4.4_2	3.3	243	320	1.22	1.06
TM-15	4.30	4.1_0	3.8_5	281	295	1.13	1.10
TM-20	4.40	4.0	--	305	--	1.08	--
TM-25	4.50	3.7	--	320	--	1.07	--
TM-40	4.80	2.8	--	365	--	0.97	--
TM-70	5.40	<1.5	--	410	--	0.49_0	--
Pure Mo	6.00	<1.5	--	470	--	0.35_6	--

Recognizing that the conjoint χ and γ data contribute to a calculation of $n(E_F)$, the numerical final results of the above semi-empirical procedure may be summarized (Table I) as sets of values of T_c, Θ_D and $n(E_F)$. The latter pair of parameters will be referred

to again in II, while T_c for β-Ti-Mo is plotted in Figure 2(b); and again in Figure 7 for comparison with the $\bar{z}$ -dependence of T_c for transition-metal-binary (T_1-T_2) alloys of the second long period. The present work provides a rationale for the characteristic double-humped shape[21], which is also exhibited by the T_c-$\bar{z}$ curves for the first-period and fifth-period transition-metal binaries. For Ti-Mo we have shown the maximum in T_c to be induced by ω-phase precipitation taking place below $\bar{z} \approx 4.3$; a regime, moreover, in which all T_1-T_2 alloys exhibit such precipitation. We, therefore, suggest that the low-$\bar{z}$ maxima present in the T_c curves for 3d-3d, 4d-4d, and 5d-5d T_1-T_2 alloys are strongly, if not entirely, contributed to by such precipitation. Secondly, it is highly significant that the other set of T_c maxima occur near $\bar{z} \approx 6.7$, the upper limit[22] of bcc stability. We conclude that superconductivity in T_1-T_2 alloys is favored by a bcc lattice, especially if accompanied by a high $n(E_F)$, and that the conditions for superconductivity became even more favorable as $\bar{z}$ approaches either limit of bcc stability; furthermore, that were it not for the intervention of structural change, T_c versus $\bar{z}$ would tend to be U-shaped.

3.3 Depression of the Superconducting Transition Temperature in Ti-Mo Through Thermal Aging of Precipitated ω-Phase

If ω-phase precipitation were indeed responsible for the depression of T_c in quenched Ti-Mo alloys for which $\bar{z} < 4.3$, we postulated that even greater decreases would be incurred as the precipitate developed to saturation in response to suitable moderate-temperature heat treatment. Accordingly, an alloy was selected whose composition (10 at.% Mo) placed it near the center of the $\bar{z}$ -range of interest; and magnetic susceptibility and low-temperature specific heat parameters were measured at various times during aging at 350° C. Figure 8 shows how T_c decreased continuously as the structural state of TM-10 proceeded from β towards "saturated" (or "metastable equilibrium"[23]) (β+ω). At this point it is useful to note that by following such changes in physical parameters during aging, the onset of decomposition into (α+β), if it does eventually take place, can be readily distinguished.

Focussing attention now on fully-aged (β+ω) TM-10, the conservation equation

$$\langle \Phi \rangle_{av} = f_\omega \, \Phi_\omega + (1-f_\omega) \, \Phi_\beta \, , \qquad (1)$$

(in which Φ symbolizes a property of a component phase) was first of all employed (in the format $\Phi \equiv [Mo]$, the "lever rule") to determine f_ω, the mole-fraction of ω-phase present after 880 hours at 350° C. Following Hickman[4], $[Mo]_\omega$ was set at 4.3 at.%; and guided by the

work of de Fontaine et al(23) [reproduced as the metastable-equilibrium (β+ω) diagram included in Figure 1(b)] the value of $[Mo]_\beta$ was taken as 21 at.%. Equation (1) then yielded $f_\omega = 0.64$. A re-application of the equation with $\Phi \equiv \gamma$, then enabled γ_ω and consequently $n(E_F)_\omega$ to be determined.

In order to obtain T_c(ω-TM-4.3) in which we are primarily interested here, a proximity-effect type of averaging equation of the form(25)

$$\langle T_c \rangle_{av} = \Sigma_i v_i \, n(E_F)_i \, T_{ci} / \Sigma_i v_i \, n(E_F)_i \qquad (2)$$

was employed, where v_i represents the superconductive volume fraction of the i^{th} component. Since even for the maximally aged alloy, the magnitude of $\Delta C/\gamma T_c$ was indicative of a bulk transition at T_c we assumed the ω-phase precipitate to be completely penetrated by the electron-pair wave-functions. It followed that v_ω was equal to the actual volume-fraction of ω-phase present which in turn is practically identical(4) with the mole-fraction, f_ω. From the measured $\langle T_c \rangle_{av}$ and the known values of the other quantities in Equation (2), T_c (ω-TM-4.3) was calculated and found to be 0.20 K. The relationship of this value to those for the quenched (β and β+ω) Ti-Mo alloys, is indicated in Figure 2(b), and again in Figure 3, by special points which are seen to fit nicely on smooth continuations of the experimentally-derived curves.

Figure 2(b) also shows that the previously described extrapolation procedure applied to single-phase bcc TM-4.3 yields $T_c = 5.25$ K. This demonstration with respect to TM-4.3, that a hypothetical structural transformation from β to ω would result in a 26-fold decrease in T_c, verified our initial argument that the depression in T_c exhibited by Ti-Mo alloys for $\bar{z} < 4.3$ was a result of ω-phase precipitation.

4. SUMMARY

Conditions particularly favorable for superconductivity in T_1-T_2 alloys exist near both the upper and lower limits of the regime of bcc stability. Thus, for example, as $\bar{z}$ decreases below 6.0 (a value which corresponds to maximal bcc stability) T_c first increases towards relatively high values, but then drops as the structure changes to hexagonal through ω-phase precipitation and finally martensitic transformation.

Although lower than if the structure were single-phase bcc, T_c in the α' regime is much larger than it would be if the structure were undistorted hcp, and in that sense it can be regarded as "enhanced". This enhancement, due to the operation of a "soft-phonon"

mechanism which accompanies the structural disorder characteristic of α', can also be induced in formerly (β+ω)-phase alloys by mechanical deformation to α".

Finally, that the T_c maximum occurring in Ti-Mo alloys near $\bar{z} = 4.4$ is, in fact, induced by ω-phase precipitation, has been demonstrated by two essentially independent experiments--one involving the hypothetical removal of ω-phase, and another based on a study of the decrease in T_c which accompanies ω-phase development during moderate-temperature aging. The fact that the linear dimensions of even the aged precipitate are commensurate with a coherence distance, is responsible for the bulk nature of the superconducting transition in the two-phase (β+ω) alloys.

REFERENCES

1. E. W. Collings and J. C. Ho, "The Science Technology and Application of Titanium", Proceedings of an International Conference, London, May, 1968; ed. R. I. Jaffee and N. E. Promisel, Pergamon Press Ltd. (1970) p. 331.

2. E. K. Molchanova, "Phase Diagrams of Titanium Alloys", ed. S. G. Glazunov (Daniel Davey · Company, Inc., N. Y., (1965) p. 29.

3. M. J. Blackburn and J. C. Williams, Trans, Met. Soc. AIME, 242 2461 (1968).

4. B. S. Hickman, Trans Met. Soc. AIME, 245 1329 (1969).

5. E. W. Collings and J. C. Ho, Proceedings of the 3rd Materials Research Symposium, November, 1969, "Electronic Density of States", Ed. L. M. Bennett, Nat. Bur. Stand. (U.S.) Special Publication 323, December, 1971, p. 587.

6. For example, according to Reference (3) the aging of Ti-Mo (11.6 wt.%) for 960 hours at 350° C resulted in the formation of ellipsoidal precipitates of geometries defined by a:b = 2.2 with b = 270 ± 100 Å.

7. In the appropriate units [Reference (5)] $n(E_F) = 0.212\ \gamma/(1 + 0.212\ \gamma\ V_{app})$; where $-1/V_{app}$ is the slope of the line in Figure 3.

8. E. W. Collings and J. C. Ho, Physics Letters, 29A 306 (1969).

9. J. Bardeen, L. N. Cooper, and J. R. Schrieffer (BCS), Phys. Rev. 108 1175 (1957); P. Morel, J. Phys. Chem. Solids, 10 277 (1959); F. M. Morin and J. P. Maita, Phys. Rev. 129 1115 (1963); see also Reference (5).

10. See Table I of Reference (14).

11. B. T. Matthias, V. B. Compton, H. Suhl, and E. Corenzwit, Phys. Rev. 115 1597 (1959).

12. B. T. Matthias, in "Superconductors", Ed. M. Tanenbaum and W. V. Wright, Interscience Publishers, 1962, p. 1.

13. B. T. Matthias, Proceedings of the 8th International Conference on Low Temperature Physics, London, 1962, Ed. R. O. Davies, Butterworths, 1963, p. 135.

14. E. W. Collings and J. C. Ho, Phys. Rev. 1 4289 (1970).

15. J. C. Ho and E. W. Collings, J. App. Phys. 42 5144 (1971).

16. E. W. Collings, J. D. Boyd, and J. C. Ho, Proceedings of the 12th International Conference on Low Temperature Physics, Kyoto, Japan, September, 1970, p. 316.

17. W. L. McMillan, Phys. Rev., 167 331 (1968).

18. J. W. Garland, K. M. Bennemann, and F. M. Mueller, Phys. Rev. Letters, 21 1315 (1968).

19. J. C. Ho and E. W. Collings, Physics Letters, 29A 206 (1969).

20. We refer to single-phase-bcc alloys, at room temperature, in the composition range 0-15 at.% Mo as "unstable"; and divide them into two classes: those in the range 5 < at.% Mo < 15, which although normally unstable do not yield unphysical elastic moduli, we designate "virtual" β-Ti-Mo; while those below the M_s composition (4-1/2 at.% Mo) we refer to as "absolutely unstable", since for these the extrapolated elastic constants yield $c_{11} < c_{12}$. Data obtained by extrapolation into this latter region must be interpreted with considerable caution.

21. B. T. Matthias, American Scientist, 58 80 (1970).

22. F. Heiniger, E. Bucher, and J. Muller, Phys. kondens. Materie, 5 243 (1966)--see in particular Figures 2 and 3.

23. D. de Fontaine, N. E. Paton, and J. C. William, Acta Met., 19 1153 (1971).

24. E. W. Collings and J. C. Ho, "Experimental Studies of Proximity-Effect-Induced Depression of the Superconducting Transition Temperatures of Two-Phase Ti-Mo Alloys"--in preparation.

25. See, for example, E. A. Lynton, "Superconductivity", Methuen and Company, 2nd Ed., 1964, pp. 150-152.

LIST OF FIGURES

Figure 1. Equilibrium and nonequilibrium phase diagrams for Ti-Mo.

Figure 2. (a) Microstructural states of quenched (from $\lesssim 1000^{\circ}C$) Ti-Mo alloys. (b), (c), and (d) Superconducting transition temperature, T_c; magnetic susceptibility, χ; and electronic specific-heat coefficient, γ, for Ti-Mo in various microstructural states.

Figure 3. Plot of log (T_c/θ_D) versus $(0.212\ \gamma)^{-1}$ [i.e., a BCS-Morel-Morin-Maita[9] plot] for Ti-Mo in various structural states.

Figure 4. Superconducting transition temperatures of both Ti-Mo and Ti-Fe plotted as functions of the electron-to-atom ratio, @.

Figure 5. Influence of deformation on the superconducting transition in Ti-Mo (5 at.%).

Figure 6. Low-temperature specific-heat data for several (β+ω)-phase Ti-Mo alloys. These alloys exhibit sharp, bulk, superconducting transitions.

Figure 7. @ -dependence of the superconducting transition temperatures of Ti-Mo alloys, compared with that of transition-metal-binary alloys of the second long period.

Figure 8. Influence of microstructural change through aging on the superconducting transition temperature of a Ti-Mo (10 at.%) alloy. The inset, based on Figure 2(b), indicates that for single-phase β-Ti-Mo (10 at.%) $T_c \approx 4.4$ K. The main figure shows this value to be consistent with those observed in the (β+ω)-phase alloys as a function of aging.

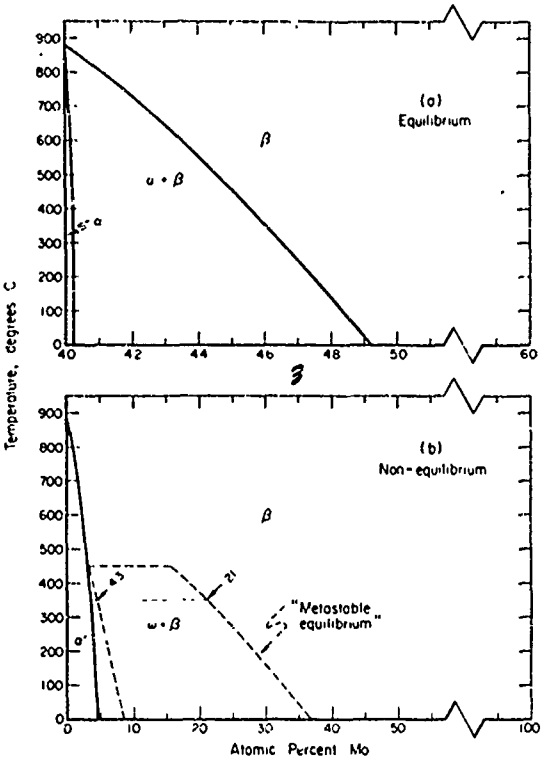

FIGURE 1. Equilibrium and non-equilibrium phase diagrams for Ti-Mo

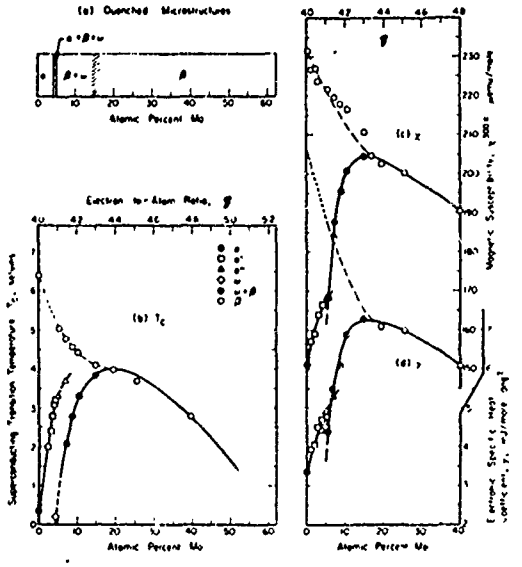

FIGURE 2. (a) Microstructural states of quenched (from $\lesssim$ 1000°C) Ti-Mo alloys. (b), (c), and (d) Superconducting transition temperature, T_c; magnetic susceptibility, χ; and electronic specific-heat coefficient, γ, for Ti-Mo in various microstructural states

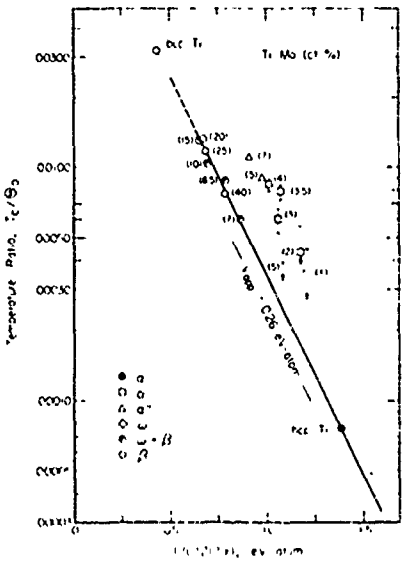

FIGURE 3. Plot of log (T_c/Θ_D) versus $(0.212\ \gamma)^{-1}$ [i.e., a BCS-Morel-Morin-Maita(9) plot] for Ti-Mo in various structural states

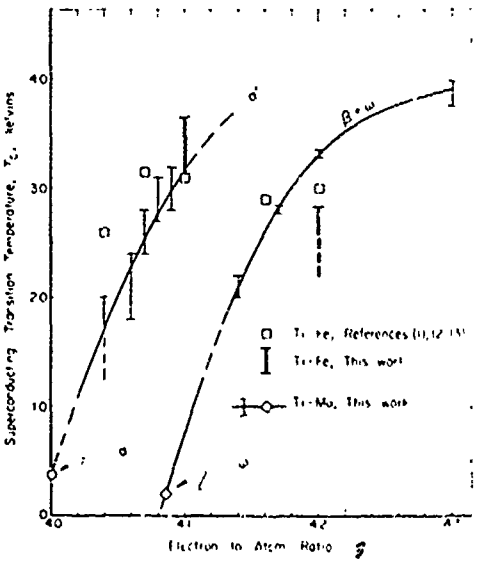

FIGURE 4. Superconducting transition temperatures of both Ti-Mo and Ti-Fe plotted as functions of the electron-to-atom ratio, z

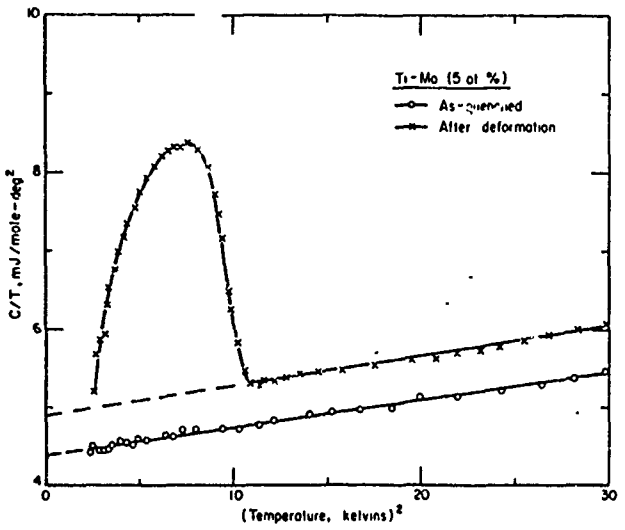

FIGURE 5. Influence of deformation on the superconducting transition in Ti-Mo (5 at.%)

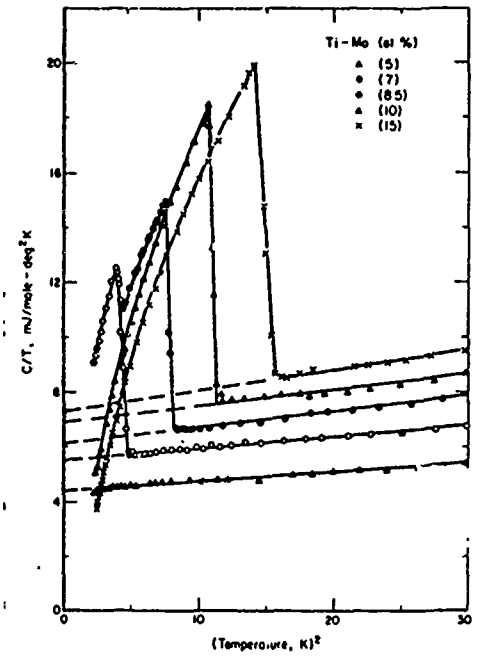

FIGURE 6. Low-temperature specific-heat data for several (β+ω)-phase Ti-Mo alloys. These alloys exhibit sharp, bulk, superconducting transitions

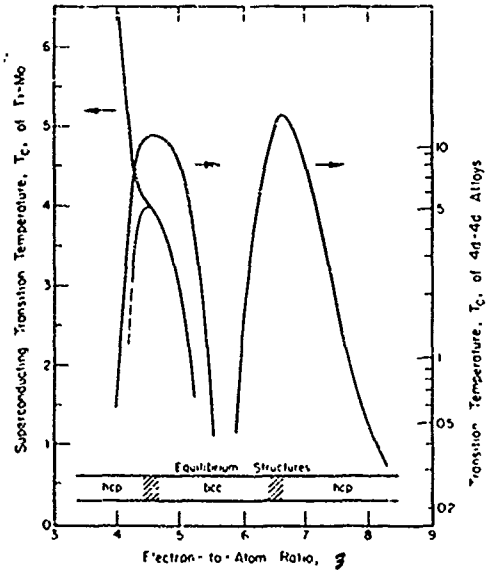

FIGURE 7. e-dependence of the superconducting transition temperatures of Ti-Mo alloys, compared with that of transition-metal-binary alloys of the second long period

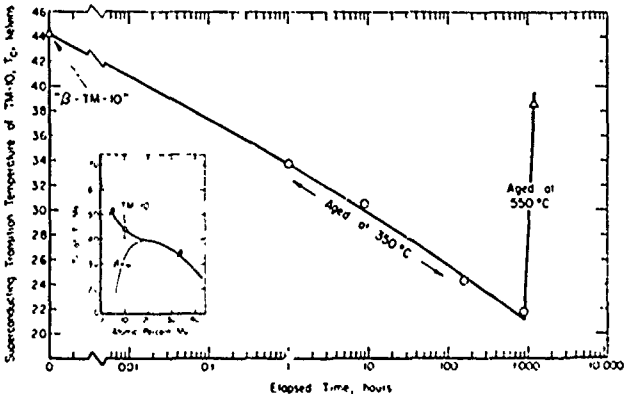

FIGURE 8. Influence of microstructural change through aging on the superconducting transition temperature of a Ti-Mo (10 at.%) alloy. The inset, based on Figure 2(b), indicates that for single-phase β-Ti-Mo (10 at.%) $T_c \lesssim 4.4$ K. The main figure shows this value to be consistent with those observed in the (β+ω)-phase alloys as a function of aging

PHYSICS OF TITANIUM ALLOYS-II: FERMI DENSITY-OF-STATES PROPERTIES, AND PHASE STABILITY OF Ti-Al AND Ti-Mo

by

E. W. Collings, J. C. Ho, and R. I. Jaffee

BATTELLE
Columbus Laboratories
Columbus, Ohio, USA, 43201

PHYSICS OF TITANIUM ALLOYS*-II: FERMI DENSITY-OF-STATES PROPERTIES, AND PHASE STABILITY OF Ti-Al AND Ti-Mo

E. W. Collings, J. C. Ho†, and R. I. Jaffee
BATTELLE
Columbus Laboratories
Columbus, Ohio 43201

The results of magnetic and calorimetric measurements leading to evaluations of the Fermi densities-of-states, $n(E_F)$ and Debye temperatures, Θ_D, of Ti-Al and Ti-Mo alloys in various structural states are presented. Phase stability in these systems is correlated with the observed variations of $n(E_F)$ and Θ_D with electron-to-atom ratio, $\bar{e}$; and the paper concludes with some general comments on the relationships between physical properties and phase stability in transition-metal binary alloys, and Ti-base alloys in particular.

*Supported by the Air Force Materials Laboratory, WPAFB, Ohio, under Contract AF33(615)69-C-1594; and the U. S. Air Force Office of Scientific Research (AFSC) under Grant No. 71-2084.

†Present address: Department of Physics, Wichita State University, Wichita, Kansas, 67208.

1. INTRODUCTION

1.1 Specimen Materials - Experimental Techniques

In an investigation of the electronic bases of phase stability and solid-solution strengthening in Ti alloys, physical property measurements were made on specimens of Ti-Al and Ti-Mo alloys as typical examples of "α-stabilized" and "β-stabilized" systems, respectively. Although a great deal of useful information was derived from measurements of a pair of electrical transport properties viz. resistivity[1], and Hall coefficient[2], the principal experimental techniques used in the study were low-temperature calorimetry augmented by magnetic susceptibility.

The low-temperature specific heat, $C = \gamma T + \beta T^3$, when plotted in the format C/T vs T^2 yields as intercept, the electronic specific heat coefficient γ [leading to $n(E_F)$, the Fermi density-of-states] and as slope ($\beta \propto \Theta_D^{-3}$) the Debye temperature Θ_D. Also, as discussed in the companion paper (henceforth I) if the specimens become superconducting within the temperature range of the calorimeter, the specific heat measurements yield a wealth of information regarding the superconducting transition. Magnetic susceptibility, χ, was used as adjunct to the low-temperature specific heat investigations. Since χ contains a separable component, χ_{spin}, which also depends on $n(E_F)$ the magnetic susceptibility technique was used to confirm and extend the results of the calorimetric measurements. Magnetic susceptibility is a simple, rapid, and economical measurement, requiring only relatively small specimens (100 mg compared with ~30g for specific heat). It can be employed advantageously when a detailed study is required of the response of $\langle n(E_F) \rangle_{av}$ to a wide range of alloy solute concentrations and heat treatments (such as quench temperatures and aging conditions). In addition the susceptibility technique can be used to investigate the $n(E_F)$ properties of alloy phases stable only at elevated temperatures and, therefore, inaccessible to low-temperature calorimetry.

1.2 Experimental Program

(a) The results of magnetic susceptibility and low-temperature specific heat measurements on "β-quenched" Ti-Mo alloys; and "α-quenched", and otherwise heat-treated, Ti-Al alloys were presented in the previous International Titanium Conference.[3] (b) In order to determine the $n(E_F)$ behavior of single-phase-bcc (i.e., β) Ti-Mo alloys in the electron-to-atom-ratio ($\mathcal{Z}$) range below about 4.3, in which they are not stable at ordinary temperatures, use was made of elevated-temperature magnetic susceptibility data in the manner indicated in the companion paper (I). A comparison of the results with those for the as-quenched alloys showed that $\langle n(E_F) \rangle_{av}$ was relatively low in the latter due to the presence of ω-phase precipitates.

(c) As confirmation of this conclusion, and in order to determine some of the physical properties of ω-phase itself, magnetic and calorimetric measurements were made as a function of ω-phase development to "metastable equilibrium"[4] through moderate-temperature (350° C) aging.

1.3 Data Analysis

An aim of the analytical procedure was to determine $n(E_F)$, a fairly fundamental quantity, and one which may be compared with the results of band structure calculations when such information is available. In suitable units[5] $n(E_F) \cong 0.212\ \gamma/(1 + 0.212\ \gamma\ V_{app})$, where the denominator is the electronic-specific-heat electron-phonon enhancement factor. When dealing with a family of transition-metal alloy superconductors the calorimetric data itself may contain sufficient information which, if expressible in the form of a linear $\log (T_c/\Theta_D)$ vs $(0.212\ \gamma)^{-1}$ plot of slope $-1/V_{app}$, enables the electron-phonon correction to be readily applied.[6] Such was, in fact, the case for Ti-Mo alloys, including α-Ti, as has already been shown[7]. Values of $n(E_F)$ [$\cong 0.212\ \gamma/(1 + 0.212\ V_{app}\ \gamma)$], calculated by applying the electron-phonon correction with $V_{app} = 0.26$ eV-atom,

Table I. Debye Temperature, Θ_D, And Fermi Density-of-States, $n(E_F)$, For Alloys in Electron-to-Atom-Ratio ($\mathcal{Z}$) Ranges $3.63 \leq$ " $\mathcal{Z}$ " ≤ 4.08 And $6.05 \leq \mathcal{Z} \leq 6.76$

Alloy*	" $\mathcal{Z}$ "	Phase	Θ_D	$n(E_F)$	Alloy	$\mathcal{Z}$	Phase	Θ_D	$n(E_F)$
HP-37	3.63	[α2]	495	0.50_1	Pure Ti	4.00	α	420	0.60
HP-33.3	3.66	[α2]	506	0.48_2	TM-4.3	4.08	ω	420	0.54_6
HP-30	3.70	[α2]	485	0.45_6					
HP-28	3.72	[α2]	518	0.41_6	MR-5	6.05	β	450	0.38_4
HP-25	3.75	α2	495	0.36_8	MR-10	6.10	β	440	0.45_0
HP-23	3.77	α2	485	0.30_3	MR-20	6.20	β	420	0.59_6
HP-20	3.80	α2	485	0.35_4	MR-25	6.25	β	405	0.62_6
HP-15	3.85	α	442	0.64_4	MR-30	6.30	β	395	0.63_4
HP-13	3.87	α	445	0.66_0	MR-40	6.40	β	340	0.67_1
HP-10	3.90	α	413	0.64_0	MR-50	6.50	β	320	0.66_4
HP-5	3.95	α	427	1.62_8	MR-58	6.58	σ	351	0.54_0
HP-3	3.97	α	413	0.61_8					
HP-2	3.98	α	403	0.61_5	MO-38	6.76	σ	371	0.54_2

*HP, TM, MR, and MO-x represent Ti-Al, Ti-Mo, Mo-Re, and Mo-Os (x at.%) respectively.

to the measured γ's for β-phase and $(\beta+\omega)$-Ti-Mo alloys have been presented in Table I of I. Also tabulated there are the directly-measured values of Θ_D, together with a list of extrapolated Θ_D's for "unstable"(8) β-Ti-Mo ($0 < \bar{z} < 4.3$), derived from a set of T_c/Θ_D values(9). The α-Ti-Al alloys on the other hand were "nonsuperconducting" (i.e., $T_c < 1.5$ K). But since pure α-Ti was represented by a point on the above-mentioned semilog plot, $V_{app} = 0.26$ eV-atom was also used in correcting γ_{Ti-Al} for electron-phonon effects. The values of $n(E_F)$ so obtained are listed (together with the directly-measured Θ_D's) in Table I of this paper.

2. RESULTS AND DISCUSSION

2.1 Physical Properties of α-, and α_2-Ti-Al and ω-, $(\beta+\omega)$-, and β-Ti-Mo Alloys

The experimental results, expressed in terms of the physical properties γ, χ, and Θ_D for α, α_2, ω, $(\beta+\omega)$, and β-phase alloys, are summarized in Figure 1.

2.1.1 Θ_D in Ti-Mo

Since as described in I, the Debye temperatures were separated out from a set of empirically-derived (T_c/Θ_D)-values, some confirmation of the validity of the form of the resulting composition-dependence of Θ_D was warranted.

Accordingly a comparison was made with Θ_D(Ti-Cr), calculated by applying Anderson's method(10), to Fisher and Dever's(11) measured elastic constants. The results of this procedure are summarized in Figure 2. Taking into consideration the fact that, in the fairly massive ingots measured, ω-phase seemed to make its appearance in Ti-Mo at a higher $\bar{z}$ than was the case for Ti-Cr(12) Figure 2(c) shows that the deduced Θ_D-composition-dependence for "virtual"(8) β-Ti-Mo was in good accord with that calculated for virtual β-Ti-Cr. Θ_D is sensitive to the shear modulus $C' = (c_{11}-c_{12})/2$ which as pointed out by Fisher and Dever(11) decreases relatively rapidly with decreasing $\bar{z}$ upon entering the virtual-β regime. This behavior is reflected in Figure 2(c). For Ti-Cr, martensitic transformation which has been observed within $4.10 < \bar{z} < 4.12$(13) seems to be related to the vanishing of C' which Figure 2(a) shows as occurring at Ti-Cr(5.03 at.%) or $\bar{z} = 4.1$. At the same time, Anderson's formula yields $\Theta_D = 208$ K; a value which tends to confirm the independently deduced behavior of Θ_D (Ti-Mo) which drops to 207 K at 5 at.% Mo, just prior to martensitic transformation at 4-1/2 at.% Mo(14). Whereas the martensitic transformation is undoubtedly associated with $C' = 0$(4,11) (i.e., "softening"(15)), de Fontaine et al(4) have shown that the $\beta \rightarrow \omega$ transformation can be achieved formally by altering

the atomic force constants at constant c_{ij}. In practice, however, it seems that it is in fact a "weakening" (16) of C' (as the softening-point, C' = 0, is approached) which leads to displacement fluctuations(4) of sufficient amplitude to excite the $\beta \rightarrow \omega$ diffusionless transformation.

2.2 Physical Properties of ω-Phase in Ti-Mo

In an aging study, Ti-Mo (10 at.%) (TM-10) was annealed at 350°C for 880 hours, by which time it was assumed that a condition approximating quasi-equilibrium had been attained as represented by the metastable phase diagram of Reference (4). The evaluation of f_ω, the mole-fraction of ω-phase present in the aged TM-10 has been discussed in I. If Φ is then taken to represent the physical properties χ, γ, and Θ_D in turn, the conservation equation:

$$\langle \Phi \rangle_{av} = f_\omega \Phi_\omega + (1-f_\omega)\, \Phi_\beta \ , \qquad (1)$$

together with the previously estimated values of Φ_β, may be used to determine χ_ω, γ_ω, and $\Theta_{D,\omega}$ for ω-TM-4.3. The values so obtained, plotted as special points in Figure 1, are seen to be in excellent agreement with the directly measured quantities for (β+ω)-Ti-Mo. These results serve to confirm that the decreases in χ and γ with decreasing $\mathcal{Z}$ ($\lesssim 4.3$) as well as the corresponding stiffening of Θ_D are, in fact, due to the continuously increasing influence of ω-phase precipitation. The $n(E_F)$ for ω-TM-4.3, derived from γ_ω using V_{app} = 0.26 eV-atom as before, is listed in Table 1.

2.3 $n(E_F)$ and Θ_D in Ti-Al and Ti-Mo

The variations of $n(E_F)$ and Θ_D with $\mathcal{Z}$, derived as a result of the magnetic and calorimetric experiments on the α and α_2 phases of Ti-Al, and the α, ω, β+ω, and β phases of Ti-Mo are shown in Figure 3. In this Figure, $\mathcal{Z}$ is not intended to have a real physical meaning but is to be interpreted as an arbitrary horizontal scale, based on the average number of atomic s, p and d electrons in the case of Ti-Al, and s+d electrons in the case of Ti-Mo. Particularly noticeable are (a): that the more stable (at say, room temperature) of a pair of allotropes, possesses the lower $n(E_F)$ together with the higher Θ_D--tightly-bound α_2-Ti-Al compared to α-Ti-Al is a very good example of this--and (b): that discontinuities or turning points in the $\mathcal{Z}$-dependence of $n(E_F)$ [or Θ_D, which scales inversely with it] occur at the limits of the various regimes of structural stability.

2.4 Phase Stability in Titanium Alloys

Figure 4 presents an experimentally-determined $n(E_F)$ curve for some binary transition-metal alloys within $4 \leq \mathfrak{z} \leq 7$. The $4 \leq \mathfrak{z} \leq 6$ regime was covered by Ti-Mo, as described above. In order to extend the range to $\mathfrak{z} = 7$, use was made of the calorimetrically determined data for Mo-Re, and Mo-Os from the work of Morin and Maita[17] and Bucher et al.[18]. In applying an electron-phonon correction in this range Morin and Maita's[17] $V_{app} = 0.42_6$ was employed. The experimentally-derived curve may be compared with a "calculated" $n(E_F)$-curve based on computed[19] values of $n(E_F)$ for bcc Ti, V, Cr, Mn, and Fe, and for the alloy system Ti-Mo[20]. Also included for comparison as an inset, are reproductions of Waber's[20] calculated n(E) profiles for the bcc 3d and 4d elements Cr and Mo. Such curves for all bcc 3d transition elements as well as some bcc 4d transition elements are characterized by a pair of dominant peaks[21]. At this stage it is appropriate to point out that, even within the context of rigid-band-type behavior [as discussed in (19)], the twin main peaks of the N(E) curves of pure bcc metals (see inset) are not to be confused with those apparent in the calorimetrically-derived $n(E_F)$ loci. The latter occur "closer in" and are induced by structural transformations of the β-phase, which take place both for $\mathfrak{z} \lesssim 4.3$ and $\mathfrak{z} \gtrsim 6.7$. Thus, the experimentally-determined maxima (e.g. that for $\mathfrak{z} \sim 4.3$) vanish when $n(E_F)$ is extrapolated semi-empirically into the unstable β regime.

De Fontaine[22] in studying the lattice dynamics of the bcc structure has computed with remarkable success the instability conditions leading to spontaneous ("athermal") ω-phase formation. Presumably the upper-$\mathfrak{z}$ limit of bcc stability could also be treated in terms of atomic force constants. The ions of course interest via the electrons[23], but so far a rigorous electronic interpretation of transition-metal-alloy phase stability, using modern theories of metals, has not yet appeared. Figures 3 and 4, however, contain some empirical results which could perhaps serve as a starting point viz.:

(a) For a given $\mathfrak{z}$ the more stable ($\lesssim$ room temperature) of a pair of allotropes is associated with the lower $n(E_F)$. Thus, for three specific single-phase situations (Figure 3):

$$n(E_F)_{\alpha_2\text{-}Ti_3Al} < n(E_F)_{\alpha\text{-}Ti_3Al} \quad (T \lesssim 830^\circ\ C)$$

$$n(E_F)_{\alpha\text{-}Ti} < n(E_F)_{\beta\text{-}Ti} \quad (T \lesssim o\ \ C)$$

$$n(E_F)_{\omega\text{-}TM\text{-}4.3} < n(E_F)_{\beta\text{-}TM\text{-}4.3} \quad (T \lesssim 500^\circ\ C)$$

(b) As $\mathcal{Z}$ is varied, maximal bcc stability is achieved with a half-filled d-band. The decrease in stability as $\mathcal{Z}$ either increases or decreases from this position is reflected in a decreasing Θ_D. This, in turn, is the result of a weakening in $C' = (c_{11}-c_{12})/2$ which has been shown to occur in each case[24,11, respectively], and which precedes structural transformation to σ-phase on one hand, and ω-phase on the other.

For Ti-base alloys, therefore, since the only way to increase the occupancy of the d-band is to add conduction electrons, transition elements tend to be β-stabilizers. On the other hand non-transition metals such as Al, Ga, and Sn reduce the occupancy of the Ti d-band, not only because they possess fewer conduction electrons but through the formation of bound states. These are, of course, α-stabilizers.

References

1. J. C. Ho and E. W. Collings, "Anomalous Electrical Resistivity in Titanium Molybdenum Alloys", Acta. Met.,---submitted for publication.

2. J. C. Ho, P. C. Gehlen, and E. W. Collings, Solid State Comm. 7 511 (1969).

3. E. W. Collings and J. C. Ho, "The Science Technology and Application of Titanium", Proceedings of an International Conference, London, May, 1968; ed. R. I. Jaffee and N. E. Promisel, Pergamon Press Ltd. (1970) p. 331.

4. D. de Fontaine, N. E. Paton, and J. C. William, Acta Met., 19 1153 (1971).

5. The units of $n(E_F)$ are taken to be states/eV-atom considering a single spin direction (i.e., half the total density-of-states); and those of γ are mJ/mole-deg^2 K.

6. E. W. Collings and J. C. Ho, phys. stat. sol. (b) 43 K123 (1971).

7. See Figure 3 of Paper I.

8. Referring to single-phase-bcc (β) Ti-Mo we have designated several electron-to-atom-ratio ($\mathcal{Z}$) regimes as follows:
   $0 \leq \mathcal{Z} \leq 4.3$ - "unstable"; a regime which includes
   (i) $0 \leq \mathcal{Z} \leq 4.05$ - "absolutely unstable", and
   (ii) $4.05 \leq \mathcal{Z} \leq 4.3$ - "virtual".

9. E. W. Collings, J. C. Ho, and R. I. Jaffee "Superconducting Transition Temperature, Lattice Instability, and Electron-to-Atom Ratio in Transition Metal Binary Solid Solutions", Phys. Rev.--to be published.

10. O. S. Anderson, J. Phys. Chem, Solids, 24 909 (1963).

11. E. S. Fisher and D. Dever, Acta Met., 18 265 (1970).

12. The microstructures of quenched Ti-Cr and Ti-Mo are reviewed in Appendix 3 of Reference (9).

13. P. Duwez and J. L. Taylor, Trans. ASM, 44 495 (1952).

14. E. W. Collings and J. C. Ho, Phys. Rev. B, 1 4289 (1970).

15. Whereas a significant decrease in C' might reasonably be referred to as "softening", Fisher and Dever(16) would refer to this as "weakening"; while de Fontaine et al.(4) reserve the term "softening" for $C' \to 0$.

16. E. S. Fisher and D. Dever, "The Science Technology and Application of Titanium", Proceedings of an International Conference, London, May, 1968; ed. R. I. Jaffee and N. E. Promisel, Pergamon Press Ltd. (1970) p. 373.

17. F. J. Morin and J. P. Maita, Phys. Rev., 129 1115 (1963).

18. E. Bucher, F. Heiniger, and J. Muller, Phys. kondens. Materie, 2 210 (1964).

19. E. C. Snow and J. T. Waber, Acta Met., 17 623 (1969).

20. J. T. Waber, in discussion to G. Broden et al., Proceedings of the 3rd Materials Research Symposium, "Electronic Density of States", Nat. Bur. Stand. (U.S.), Spec. Pub. 323, December, 1971, p. 217 (pp. 221-223).

21. The n(E) profiles for Nb and Mo possess less-pronounced centrally-situated peaks; a property which seems to show up in the calculated n(E_F) curve for Ti-Mo alloys, but which is not shared by the experimentally observed n(E_F) for Ti-Mo.

22. D. de Fontaine, Acta Met., 18 275 (1970).

23. M. H. Cohen in "Alloying Behavior and Effects in Concentrated Solid Solutions", T. B. Massalski (ed.) Gordon and Breach (1965) pp. 1-23; A. Blandin, loc. cit. pp. 50-84; W. A. Harrison, "Pseudopotentials in the Theory of Metals", W. A. Benjamin, Inc. (1966).

24. D. L. Davidson and F. R. Brotzen, J. App. Phys., 39 5768 (1968)

LIST OF FIGURES

Figure 1. Composition-dependences of magnetic susceptibility (χ), low-temperature-specific-heat coefficient (γ), and Debye temperature (Θ_D), for Ti-Al and Ti-Mo alloys in various structural states viz.: α_2, α (Ti-Al); and α, ω, $\omega+\beta$, and β (Ti-Mo).

Figure 2. (a) Elastic constants c_{11}, c_{12} and c_{44} of Ti-Cr - after Fisher and Dever(11,16). (b) Θ_D for Ti-Cr calculated from the data of the previous figure, using Anderson's(10) method. (c) Comparison of the temperature-dependence of Θ_D for Ti-Cr and Ti-Mo. At the observed room-temperature threshold of martensitic transformation for Ti-Mo (viz. 4-1/2 at.%), and when $c_{11} = c_{12}$ for Ti-Cr, we find $\Theta_D]_{Ti\text{-}Mo} \tilde{=} \Theta_D]_{Ti\text{-}Cr} = 208$ K.

Figure 3. Empirically-derived Fermi density-of-states, $n(E_F)$, and Debye temperature, Θ_D, as functions of electron-to-atom ratio, z, in Ti-base alloys.

Figure 4. z-dependence of $n(E_F)$ for transition-metal-binary (i.e. T_1-T_2) alloys: (a) Empirically-derived curve for Ti-[illegible]-Re, based on the present data and those of References (17) and (18); (b) "calculated" $n(E_F)$ for bcc T_1-T_2 alloys based on published data points(19) for bcc Ti, V, Cr, Mn and Fe. For comparison, the z-dependence of Θ_D for Ti-Mo-Re is also shown. The remarkable inverse scaling exhibited by the $n(E_F)$ and Θ_D curves owes its origin to phase stability considerations.

Inset are calculated n(E) curves for bcc Ti and Mo from the work of Waber and colleagues(20). $n(E_F)$ is at a local minimum in n(E) for both bcc Ti and Mo; however, the latter shows an extra peak, which seems to be reflected in the calculated $n(E_F)$ for Ti-Mo(20) but not in the experimentally derived curve presented here.

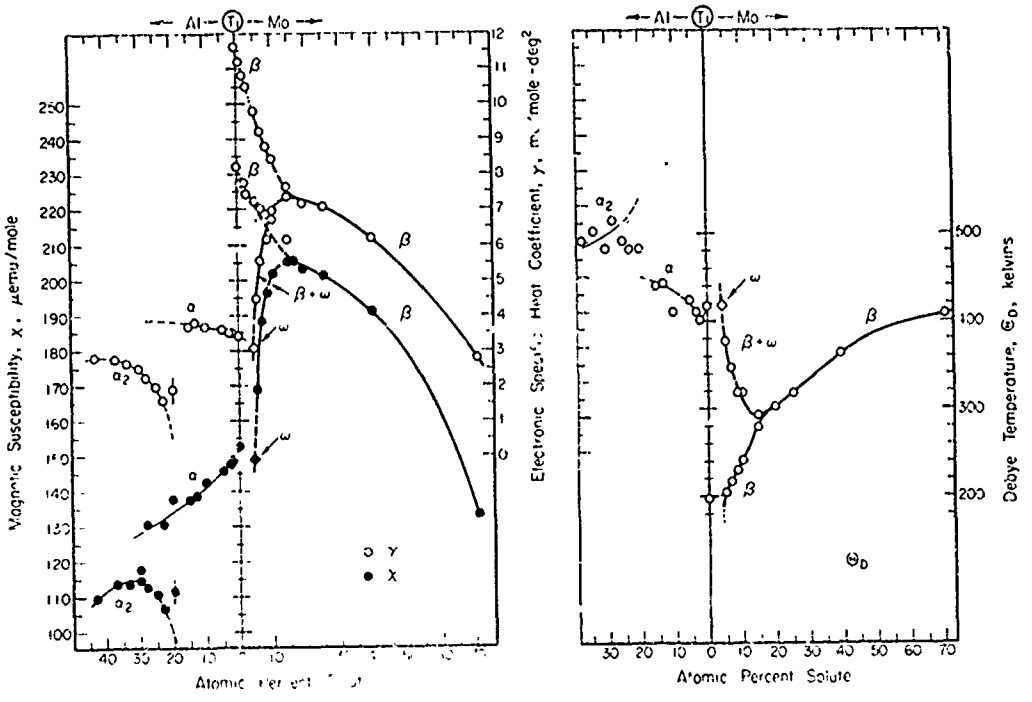

Figure 1. Composition-dependences of magnetic susceptibility (χ), low-temperature-specific-heat coefficient (γ), and Debye temperature (Θ_D), for Ti-Al and Ti-Mo alloys in various structural states viz.: α_2, α (Ti-Al); and α, ω, $\omega+\beta$, and β (Ti-Mo).

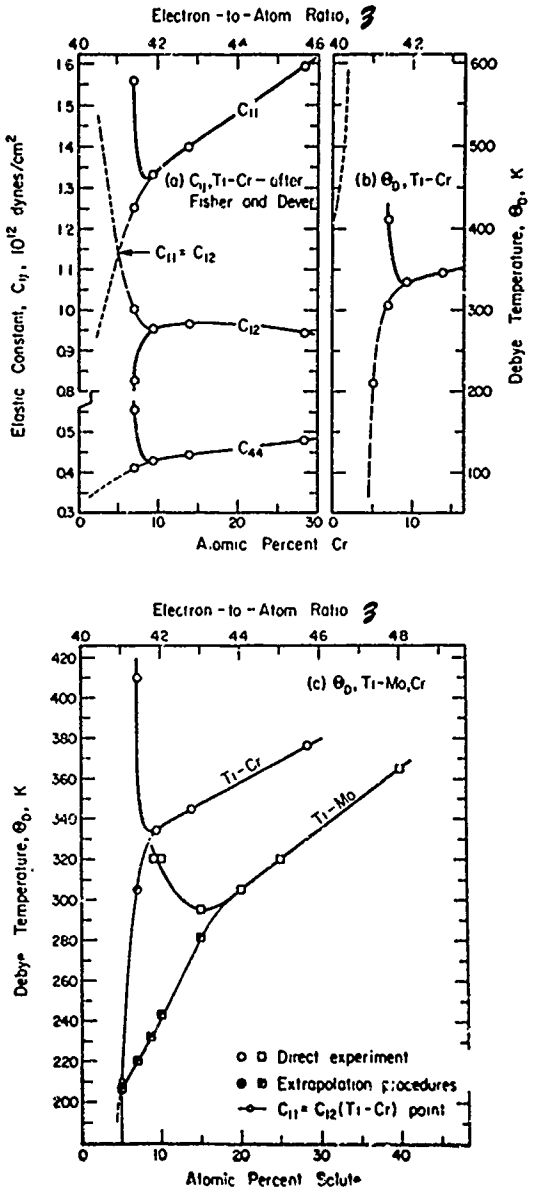

Figure 2. (a) Elastic constants c_{11}, c_{12} and c_{44} of Ti-Cr - after Fisher and Dever(11,16). (b) Θ_D for Ti-Cr calculated from the data of the previous figure, using Anderson's(10) method. (c) Comparison of the temperature-dependence of Θ_D for Ti-Cr and Ti-Mo. At the observed room-temperature threshold of martensitic transformation for Ti-Mo (viz. 4-1/2 at.%), and when $c_{11} = c_{12}$ for Ti-Cr, we find $\Theta_D]_{\text{Ti-Mo}} \tilde{=} \Theta_D]_{\text{Ti-Cr}} = 208$ K.

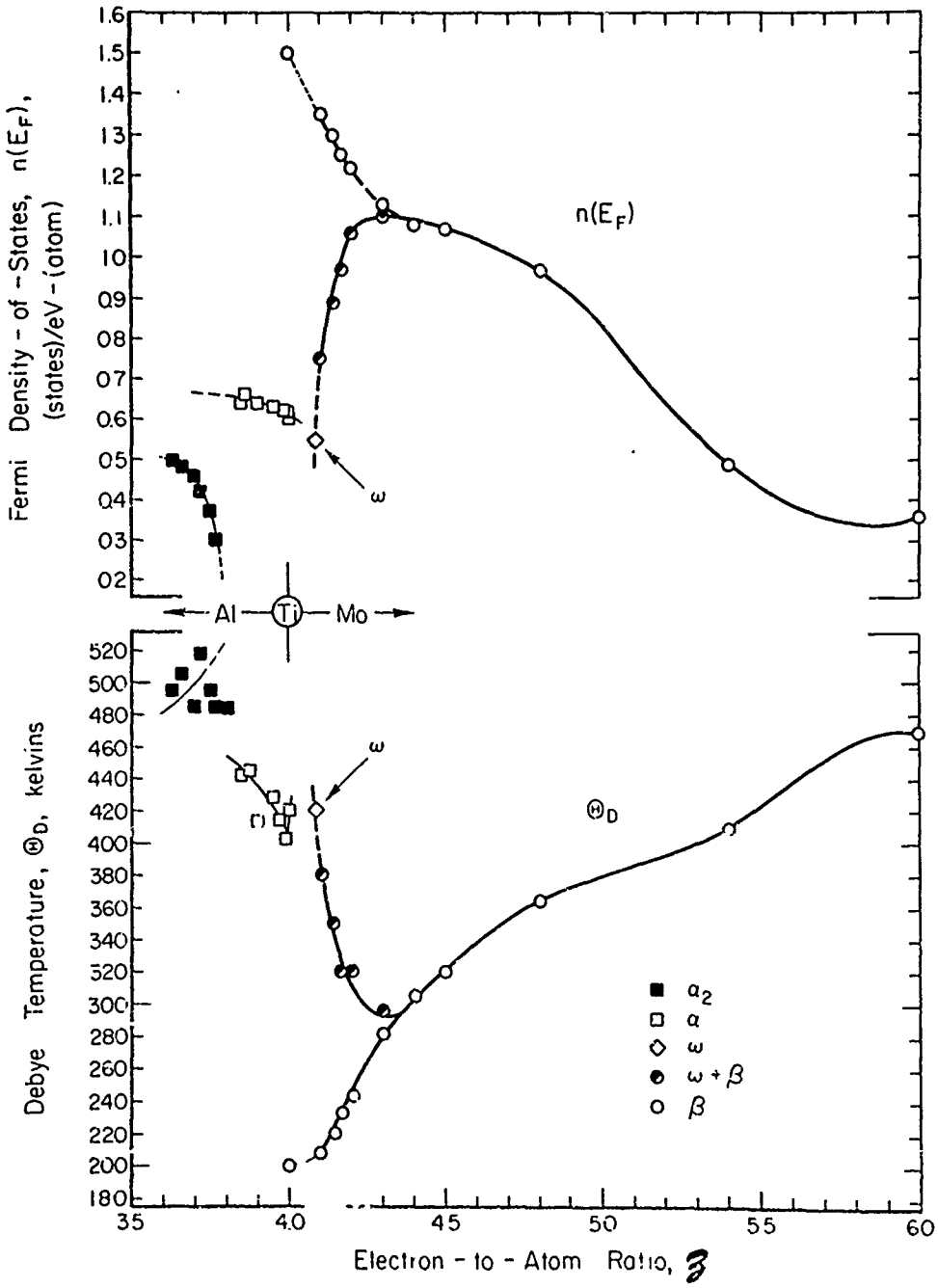

Figure 3. Empirically-derived Fermi density-of-states, $n(E_F)$, and Debye temperature, Θ_D, as functions of electron-to-atom ratio, e/a, in Ti-base alloys.

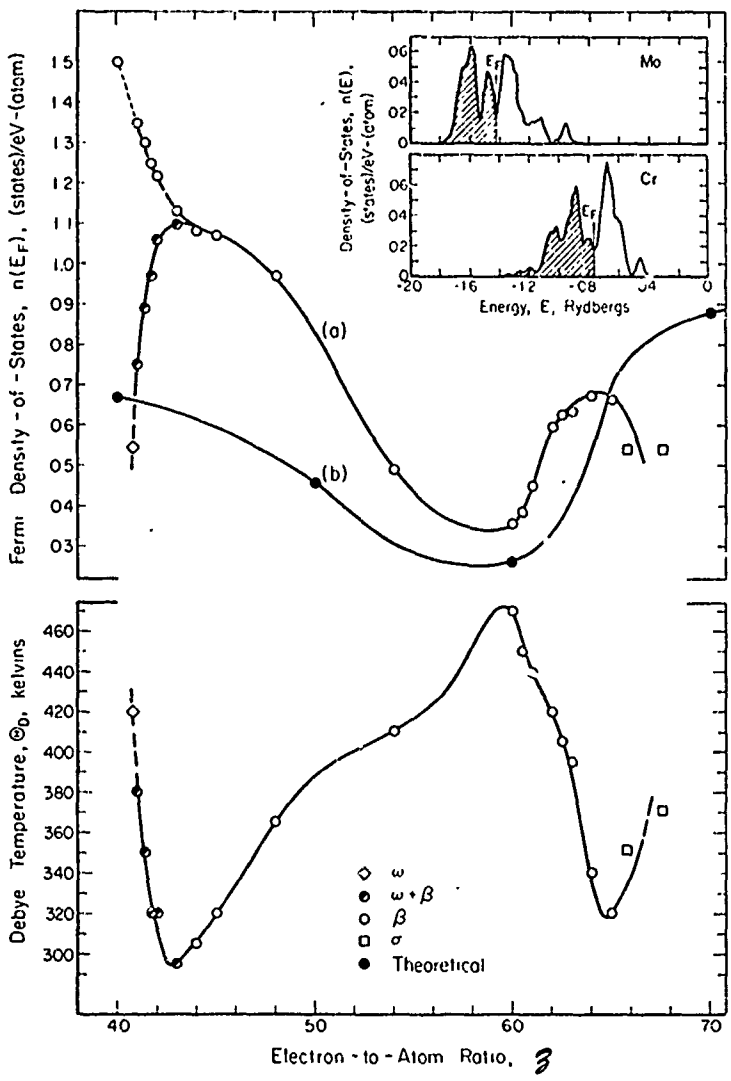

Figure 4. z-dependence of $n(E_F)$ for transition-metal-binary (i.e. T_1-T_2) alloys: (a) Empirically-derived curve for Ti-Mo-Re, based on the present data and those of References (17) and (18); (b) "calculated" $n(E_F)$ for bcc T_1-T_2 alloys based on published data points[19] for bcc Ti, V, Cr, Mn and Fe. For comparison, the z-dependence of Θ_D for Ti-Mo-Re is also shown. The remarkable inverse scaling exhibited by the $n(E_F)$ and Θ_D curves owes its origin to phase stability-considerations.

Inset are calculated n(E) curves for bcc Ti and Mo from the work of Waber and colleagues[20]. $n(E_F)$ is at a local minimum in n(E) for both bcc Ti and Mo; however, the latter shows an extra peak, which seems to be reflected in the calculated $n(E_F)$ for Ti-Mo[20] but not in the experimentally derived curve presented here.

THE INVERSE SCALING OF THE LOW-TEMPERATURE-SPECIFIC-HEAT PARAMETERS γ AND Θ_D IN TRANSITION-METAL BINARY ALLOYS AND ITS DEPENDENCE ON PHASE STABILITY*

E. W. COLLINGS, Metal Science Group, BATTELLE, Columbus Laboratories, Columbus, Ohio, USA 43201

and

J. C. HO, Physics Department, Wichita State University, Wichita, Kansas, USA 67208

In low-temperature-calorimetric studies of transition-metal-binary alloys in the average group number or electron/atom ratio ($\mathcal{Z}$) range $4 < \mathcal{Z} < 7$, an inverse scaling noted in the γ and Θ_D (*versus* $\mathcal{Z}$) profiles can be rationalized in terms of the bcc binary alloy low-temperature structural phase stability.

* * * *

In studies of the low-temperature calorimetric properties of sequences of Ti-Mo alloys[1] it was noticed that suitably scaled curves of γ and Θ_D *versus* electron/atom ratio ($\mathcal{Z}$), for $4.4 \lesssim \mathcal{Z} \leq 6$, were practically mirror images of each other in a horizontal axis. Inverse trends in γ and Θ_D have been noted before, particularly by Bucher et al.[2,3] who demonstrated the existence of opposite curvatures in $\gamma(\mathcal{Z})$ and $\Theta_D(\mathcal{Z})$ for the systems V-Fe and V-Ru near $\mathcal{Z} \cong 5.7$. In Figure 1 our own calorimetric results for Ti-Mo are augmented by published data for Mo-Re[4] and a Mo-Os alloy[3]. It can be seen that the inverse scaling of γ and Θ_D prevails throughout the entire range indicated.

---

* Supported by Battelle's Columbus Laboratories; the Air Force Materials Laboratory, Wright-Patterson Air Force Base, Ohio [Contract AF33(615)69-C-1594]; and the U. S. Air Force Office of Scientific Research (AFSC) [Grant No. 71-2084].

As has already been pointed out,[3] a demonstrated[5] inverse proportionality between $n(E_F)$ and the bulk modulus of the conduction electron gas, which is equivalent to an inverse relationship between γ and Θ_D, does not lead to effects of the magnitude of those encountered here. Indeed, we suggest that the electronic bulk modulus is not primarily involved, but that the observed effect can be treated at constant volume with the elastic shear modulus $C' = (c_{11}-c_{12})/2$ as key parameter.

In Figure 1 we see that the maxima in γ occur at either limit of the regime of stability of the bcc phase at low temperatures. An electronic approach to phase stability in simple-metal alloys such as that presented recently by Stroud and Ashcroft[6] has yet to be extended to alloys involving transition elements. We have an <u>empirical</u> result[7], however, that in pure Ti, some Ti-Mo alloys, and in Ti_3Al, the more stable (at low temperatures) of a pair of allotropes has the lower $n(E_F)$. Thus, below $z \approx 4.3$, γ decreases with decreasing z as the lattice decomposes into $(\beta+\omega)$. Similarly, for $z \gtrsim 6.7$, γ drops as the structure transforms to the more stable σ-phase.

The stability of the bcc structure is greatest when the d-band is about half full, as it is in Cr (see inset, Figure 1), and decreases with either the filling or the emptying of the band. C' may be used as an indicator of bcc stability since, for example, it can be regarded as a measure of the extent to which the cubic lattice resists deformation at constant volume. Thus, Figure 1(c) shows C' to be maximal near $z \approx 5.9$ where $n(E_F)$, hence γ, is lowest. Moving in either direction from this point, γ and C' have opposite slopes in response to decreases in bcc stability. Since C' is an important component of the Anderson[8] expression for Θ_D, the variation in lattice stability about $z \approx 5.9$ is responsible

for the inverse curvatures of γ and Θ_D near that point. Finally, near either terminal of bcc stability the stiffening which accompanies the transformation away from bcc to a more stable structure (ω-phase and σ-phase respectively), causes Θ_D to increase as γ decreases.

References

(1) E. W. Collings, J. C. Ho, and R. I. Jaffee, Phys. Rev., to be published:--see also A. K. Sinha, J. Phys. Chem. Solids 29 749 (1968).

(2) E. Bucher, F. Heiniger and J. Muller, Proc. LT9 1963/64, p. 1059.

(3) F. Heiniger, E. Bucher, and J. Muller, Phys. kondens. Materie, 5, 243 (1966).

(4) F. J. Morin and J. P. Maita, Phys. Rev., 129, 1115 (1963).

(5) J. A. Rayne, Phys. Rev., 118, 1545 (1960).

(6) D. Stroud and N. W. Ashcroft, J. Phys. F:Metal Phys., 1, 113 (1971).

(7) E. W. Collings, J. C. Ho, and R. I. Jaffee, Proceedings of the Second International Conference on Titanium, Cambridge, Massachusetts, May 2-5, 1972, to be published.

(8) O. L. Anderson, J. Phys. Chem. Solids, 24, 909 (1963).

(9) E. S. Fisher and D. Dever, Acta Met., 18, 265 (1970).

(10) D. I. Bolef, J. App. Phys., 32, 100 (1961).

(11) D. I. Bolef and J. de Klerk, Phys. Rev., 129, 1063 (1963).

(12) D. L. Davidson and F. R. Brotzen, J. App. Phys., 39, 5768 (1968).

(13) F. H. Featherston and J. R. Neighbours, Phys. Rev., 130, 1324 (1963).

(14) E. C. Snow and J. T. Waber, Acta Met., 17, 623 (1969).

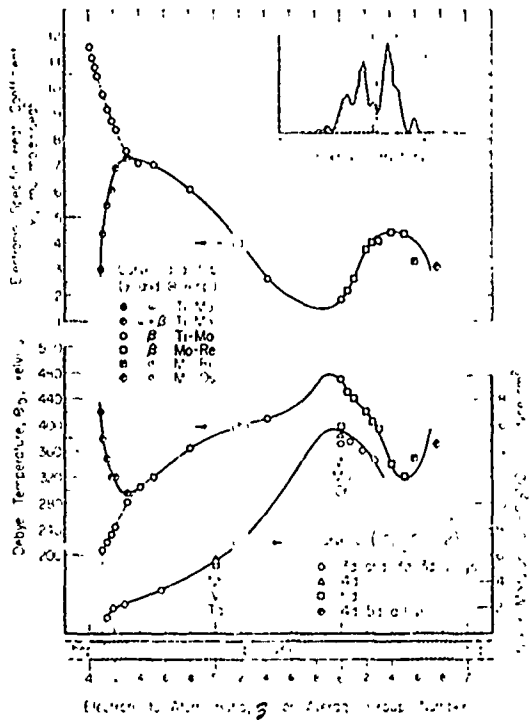

Figure 1. Curves (a) and (b): Electronic specific heat coefficient, γ, and Debye Temperature, Θ_D, respectively. The broken lines represent estimated data for bcc Ti-Mo alloys were they stable at ordinary temperatures. These and the stable bcc Ti-Mo data are from Ref. (1). The Mo-Re and Mo-Os data are from Refs. (4) and (3) resp. Curve (c): Elastic shear modulus, $(c_{11}-c_{12})/2$, for various transition metals and binary alloys. Symbols ○ refer to bcc Ti-Cr[9], V[10], and Cr[11]; the △ refer to Nb[10] and Mo[12]; the □ refer to Ta[13] and W[13]; and the ◐ refer to three Mo-Re alloys[12]. Inset is a calculated n(E) curve for bcc Cr--after Snow and Waber[14]; in it the band-structure peaks are "more widely separated" than the peaks in curve (a) which are induced by phase transformations.

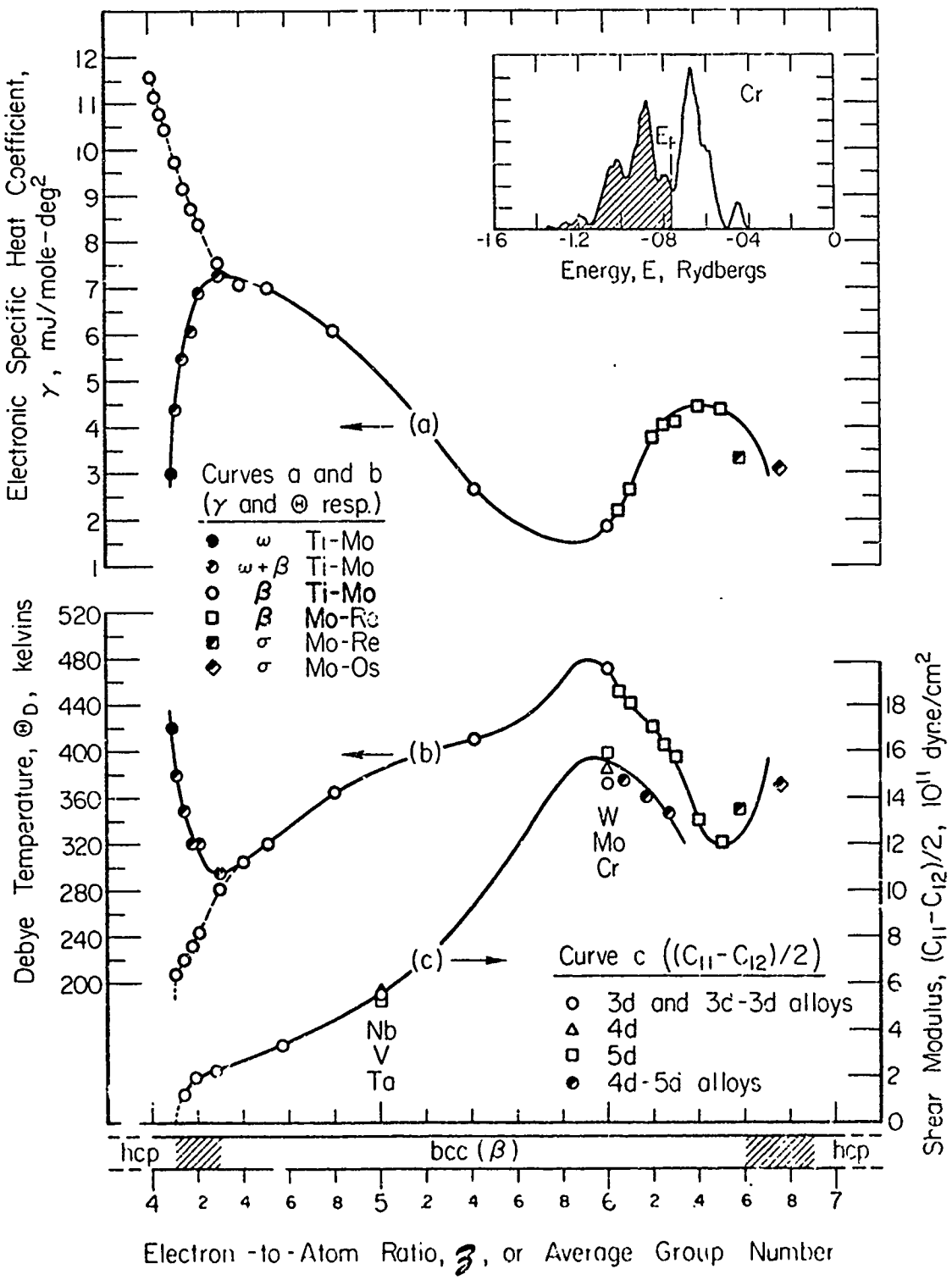
Electronic Specific Heat Coefficient, γ, mJ/mole-deg²
Cr
E_f
-16
-1.2
-08
-04
0
Energy, E, Rydbergs
(a)
Curves a and b
(γ and Θ resp.)
ω Ti-Mo
ω+β Ti-Mo
β Ti-Mo
β Mo-Re
σ Mo-Re
σ Mo-Os
Debye Temperature, Θ_D, kelvins
(b)
W
Mo
Cr
(c)
Curve c ((C11-C12)/2)
3d and 3d-3d alloys
4d
5d
4d-5d alloys
Nb
V
Ta
Shear Modulus, (C11-C12)/2, 10¹¹ dyne/cm²
hcp
bcc (β)
hcp
Electron-to-Atom Ratio, z, or Average Group Number